AMERICAN SOCIETY FOR MICROBIOLOGY | **Applied and Environmental Microbiology**®

Glycine Betaine Monooxygenase, an Unusual Rieske-Type Oxygenase System, Catalyzes the Oxidative *N*-Demethylation of Glycine Betaine in *Chromohalobacter salexigens* DSM 3043

Ya-Hui Shao,[a] Li-Zhong Guo,[a] Yu-Qing Zhang,[a] Hao Yu,[a] Bai-Suo Zhao,[b] Hai-Qiang Pang,[c] Wei-Dong Lu[a]

[a]Shandong Provincial Key Laboratory of Applied Mycology, College of Life Sciences, Qingdao Agricultural University, Qingdao, People's Republic of China
[b]Graduate School, Chinese Academy of Agricultural Sciences, Beijing, People's Republic of China
[c]Shandong Ruiying Pioneer Pharmaceutical Co., Ltd., HeZe, People's Republic of China

ABSTRACT Although some bacteria, including *Chromohalobacter salexigens* DSM 3043, can use glycine betaine (GB) as a sole source of carbon and energy, little information is available about the genes and their encoded proteins involved in the initial step of the GB degradation pathway. In the present study, the results of conserved domain analysis, construction of in-frame deletion mutants, and an *in vivo* functional complementation assay suggested that the open reading frames Csal_1004 and Csal_1005, designated *bmoA* and *bmoB*, respectively, may act as the terminal oxygenase and the ferredoxin reductase genes in a novel Rieske-type oxygenase system to convert GB to dimethylglycine in *C. salexigens* DSM 3043. To further verify their function, BmoA and BmoB were heterologously overexpressed in *Escherichia coli*, and ^{13}C nuclear magnetic resonance analysis revealed that dimethylglycine was accumulated in *E. coli* BL21(DE3) expressing BmoAB or BmoA. In addition, His-tagged BmoA and BmoB were individually purified to electrophoretic homogeneity and estimated to be a homotrimer and a monomer, respectively. *In vitro* biochemical analysis indicated that BmoB is an NADH-dependent flavin reductase with one noncovalently bound flavin adenine dinucleotide (FAD) as its prosthetic group. In the presence of BmoB, NADH, and flavin, BmoA could aerobically degrade GB to dimethylglycine with the concomitant production of formaldehyde. BmoA exhibited strict substrate specificity for GB, and its demethylation activity was stimulated by Fe^{2+}. Phylogenetic analysis showed that BmoA belongs to group V of the Rieske nonheme iron oxygenase (RO) family, and all the members in this group were able to use quaternary ammonium compounds as substrates.

IMPORTANCE GB is widely distributed in nature. In addition to being accumulated intracellularly as a compatible solute to deal with osmotic stress, it can be utilized by many bacteria as a source of carbon and energy. However, very limited knowledge is presently available about the molecular and biochemical mechanisms for the initial step of the aerobic GB degradation pathway in bacteria. Here, we report the molecular and biochemical characterization of a novel two-component Rieske-type monooxygenase system, GB monooxygenase (BMO), which is responsible for oxidative demethylation of GB to dimethylglycine in *C. salexigens* DSM 3043. The results gained in this study extend our knowledge on the catalytic reaction of microbial GB degradation to dimethylglycine.

KEYWORDS glycine betaine monooxygenase, Rieske-type oxygenase, *N*-demethylation, *Chromohalobacter salexigens* DSM 3043

Glycine betaine (*N,N,N*-trimethylglycine [GB]) is widely available in the environment and accumulated by many microbes and plants in response to environmental stress, especially to salt stress. It also plays an important role in some mammals as a source of methyl group (1). Under osmotic stress conditions, most of the microorgan-

isms accumulate GB by uptake from the environment via various transport systems in the betaine/choline/carnitine transporter (BCCT) family (2), major facilitator superfamily (MFS) (3), and/or the ATP-binding cassette (ABC) transporters located on cellular membranes, or they produce it intracellularly via choline oxidation pathway, with betaine aldehyde as the intermediate (4, 5). Moreover, some halophilic anoxygenic phototrophic bacteria, halophilic cyanobacteria, and halophilic methanogenic archaebacteria can use glycine in *de novo* synthesis of GB through the action of methyltransferases with *S*-adenosylmethionine (SAM) as a methyl donor (6, 7).

Besides acting as an organic osmolyte, GB can be used as a source of carbon, nitrogen, and energy in many bacteria. Under anaerobic conditions, GB is degraded by fermentation, reduction, or oxidation reactions to produce dimethylglycine, trimethylamine, acetate, or butyrate, etc. (8, 9). Under aerobic conditions, GB can also be catabolized by many microorganisms isolated from diverse habitats, including the members in the genera *Agrobacterium*, *Pseudomonas*, *Micrococcus*, *Streptomyces* (10), *Arthrobacter* (11), *Corynebacterium* (12), *Sinorhizobium* and other *Rhizobiaceae* (13), *Chromohalobacter* (14), and *Halomonas* (14). Moreover, Kortstee observed that all the choline-utilizing bacteria tested were capable of growth on media with GB, dimethylglycine, or sarcosine as the sole source of carbon and nitrogen, suggesting that these bacteria could aerobically decompose GB to glycine through a progressive demethylation reaction, with dimethylglycine and sarcosine as the metabolic intermediates (10). So far, two types of enzymes involved in the initial step of aerobic microbial GB catabolism have been reported. The first type is betaine-homocysteine methyltransferase (BHMT; EC 2.1.1.5), which catalyzes the transfer of a methyl group from GB to homocysteine, producing dimethylglycine and methionine. The enzyme activities were detected in the crude extracts of the species of *Pseudomonas* (15) and *Sinorhizobium* (16). In addition, Barra and colleagues identified the SMc04325 open reading frame (ORF) from *Sinorhizobium meliloti* strain 102F34 as the BHMT-encoding gene (17), and the native BHMT protein purified from *Aphanothece halophytica* was proven to be an octameric structure (18). The second type of enzyme responsible for the first step of aerobic GB catabolism was found in *Pseudomonas aeruginosa* (19) and *Pseudomonas syringae* (20). Through the strategies of transposon mutagenesis and gene disruption, the *gbcA* (PA5410) and *gbcB* (PA5411) genes were proven to be necessary for GB catabolism in *P. aeruginosa* (19), and their overexpression was shown to be sufficient to reduce intracellular GB pool (21). Bioinformatics analysis predicted that the *gbcA* and *gbcB* genes might encode a dioxygenase to remove a methyl group from GB, producing dimethylglycine and perhaps formaldehyde (19).

As a model organism for studying the mechanism of prokaryotic osmoregulation, the complete genome sequence of *Chromohalobacter salexigens* DSM 3043 had been determined by the Joint Genome Institute of the U.S. Department of Energy (22). The strain can not only use GB as the sole source of carbon and energy but also accumulate it intracellularly under high-salinity environments (14). Previous studies had shown that *C. salexigens* DSM 3043 also can grow on medium with dimethylglycine as the sole source of carbon and energy, and the disruption of sarcosine oxidase-encoding genes impairs its growth on mineral salt medium with GB as the sole carbon source (23), suggesting that GB could be aerobically catabolized to glycine by three successive demethylation reactions, with dimethylglycine and sarcosine as the intermediates. In this report, with a combination of genetic, bioinformatics, and biochemical approaches, we describe the characterization of the genetic and biochemical mechanisms for the initial step of the GB degradation pathway in the moderate halophile *C. salexigens* DSM 3043.

RESULTS

Identification of a two-gene cluster in *C. salexigens* DSM 3043. *C. salexigens* DSM 3043 can utilize GB as a sole source of carbon and nitrogen (see Fig. S1 in the supplemental material). Therefore, a BLASTP analysis of *C. salexigens* DSM 3043 (GenBank accession number NC_007963.1) was performed to identify candidate

NADH-binding domain   **Plant-type [2Fe-2S] binding domain**

(A)
```
BmoB  128 MLSGGVGVTPLMSMT 142   316 KACGMGICGTCKVKKLAGEVTMEHNGGITEEDEADGYILSCC 357
TsaB  114 LLAGGIGVTPIYAMA 128   264 WSCREGICGTCEAPVLEGEVQHLDYVLSPEERAEQRRMMVCV 305
VanB  109 LFAGGIGITPILCMA 123   264 VSCEQGICGTCITRVVDGEPDHRDFFLTDAEKAKNDQFTPCC 305
Pht2  119 FVAGGIGITPILSMM 133   273 SSCESGTCGSCRTRLIEGDVEHRDMVLREDE..QHDQIMICV 312
CbaB  117 LICGGIGITPMVHMA 131   262 SSCRQGICGMCETTLISGVPDHRDRLLTDSEKASGRTMLICC 303
PobB  117 FIAGGIGITPLWSMV 131   266 SSCQQGVCGICETAVLAGVPDHRDLVLSDQERAAGRTMMICC 307
          **  *   *                *      *   *                        *
```

FAD-binding domain

(B)
```
BmoB  65 VMRSYTISSSPSVPYSFSITVKRLPDGRVSNWLHENLQVGSELVVHGPVGDFN 117
AntC 152 DWRSYSFANRPNASNQLQFLIRLLPNGVMSNYLRERCQVGQTLIMEAPLGSFY 204
BenC 150 ATRSYSFSTGP.TSKELSFLVKITDGGLMSEYLRSRAQVGDTLEFTGPMGSFF 201
CbdC 150 ESRAYSYSSMP.GSSHVTFLVRDVPNGKMSGYLRNQATITETFTFDGPYGAFY 201
OxoR 153 VVRSYSPSSTTADVPKMEFLIRLLPGGAMSSYLQEKAAQDEVLTLSGPYGAFF 205
         *  * **                         *      *
```

Rieske [2Fe-2S] domain   **Nonheme iron domain**

(C)
```
BmoA   94 FHNVCRHRGSRLCTQAKG..KVAKLVCPYHQW 123   207 LVIENNRECYHCNGAHPE 224
GbcA   94 FHNVCRHRGSRLCVSEKG..KVAKLVCPYHQW 123   207 LVIENNRECYHCNGSHPE 224
Stc2   82 FHNSCRHRGSLICKARQG..QVAKLVCPYHQW 111   194 LVWENNRECYHCSSNHPA 211
CntA   82 FYNVCPHRGHELLSGSGK..AKNVITCPYHAW 111   198 VIVDNYMECYHCGPAHPG 215
OxyBAC 78 YHNVCPHRGSELCTADEQPLRGGRILCPYHAW 109   194 ILWENFHECLHCPGVHPS 211
          *     *            *      *            *     *     *      *
```
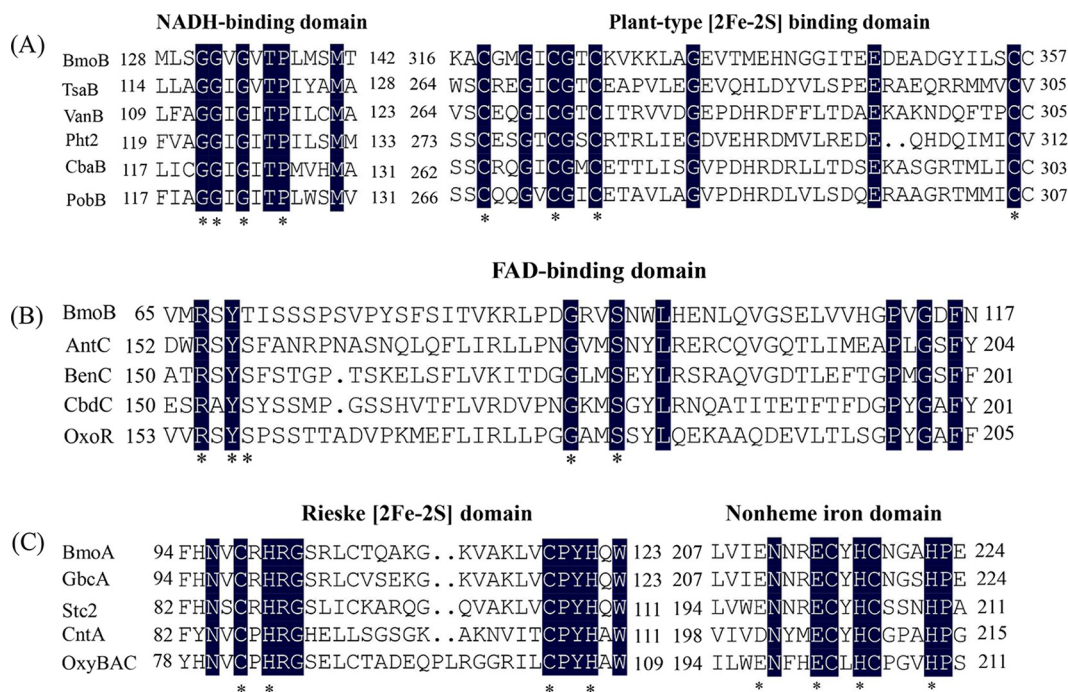
FIG 1 Conserved domain analysis of BmoA and BmoB from *C. salexigens* DSM 3043. (A) Identification of a NADH-binding domain and a plant-type [2Fe-2S] binding domain in the BmoB by amino acid sequence alignment with those of the flavin reductase components in the Rieske nonheme iron oxygenase (RO) class IA, as classified by Batie et al. (44). (B) Identification of a flavin-binding domain in the BmoB by amino acid sequence alignment with those of the flavin reductases in the RO class IB, as classified by Batie et al. (44). (C) Identification of a Rieske [2Fe-2S] domain and a nonheme Fe(II) domain in the BmoA by amino acid sequence alignment with those of the members in the RO family. Numbers represent the positions of the residues in the complete amino acid sequence of the following proteins (accession number): BmoB (499825574), a GB monooxygenase reductase component from *C. salexigens* DSM 3043; TsaB (AAC44805), a toluene sulfonate methyl-monooxygenase reductase component from *Comamonas testosteroni* T-2; VanB (O05617), a vanillate *O*-demethylase oxidoreductase from *Pseudomonas* sp. strain HR199; Pht2 (Q05182), a phthalate 4,5-dioxygenase reductase subunit from *P. putida* NMH102-2; CbaB (Q44257), a 3-chlorobenzoate-3,4-dioxygenase reductase subunit from *Alcaligenes* sp. strain BR60; PobB (Q52186), a phenoxybenzoate dioxygenase ferredoxin reductase from *Pseudomonas pseudoalcaligenes* POB310; AntC (AAC34815), an anthranilate dioxygenase reductase from *Acinetobacter* sp. strain ADP1; BenC (BAB70700), a benzoate 1,2-dioxygenase reductase from *Rhodococcus* sp. strain RHA1; CbdC (CAA55683), a 2-halobenzoate 1,2-dioxygenase reductase from *Pseudomonas cepacia* 2CBS; OxoR (CAA73201), a 2-oxo-1,2-dihydroquinoline 8-monooxygenase reductase from *P. putida* 86; BmoA (759867680), the terminal oxygenase component of GB monooxygenase from *C. salexigens* DSM 3043; GbcA (15600603), the predicted component of GB dioxygenase from *P. aeruginosa* PAO1; Stc2 (AAK65058), a stachydrine demethylase from *S. meliloti* 1021; CntA (EEX03955), the terminal oxygenase component of carnitine oxygenase from *A. baumannii* ATCC 19606; and OxyBAC (WP_068587002), benzalkonium chloride oxygenase from *Pseudomonas* sp. BIOMIG1. The amino acid residues conserved in the domains are indicated by asterisks (*), while identical amino acids residues in the aligned sequences are shown in black.

genes involved in the first step of the GB catabolism pathway using the two-gene cluster identified as *gbcAB* (PA5410 and PA5411) from *P. aeruginosa* PAO1 as the query sequences (19). Csal_1004 and Csal_1005 exhibited good homology with PA5410 (66% identity/81% similarity) and PA5411 (76% identity/84% similarity), respectively. Csal_1005 is 1,107 bp in length and encodes a predicted 368-amino-acid protein. Conserved domain analysis revealed the presence of conserved sequences for the NAD(P)H-binding domain (GGXGXXP) (Fig. 1A), the plant-type [2Fe-2S] domain (CX$_4$C X$_2$CX$_{29}$C) (Fig. 1A), and the flavin-binding domain (RXYSX$_{19-20}$GX$_2$S) (Fig. 1B) in the theoretical protein sequence of Csal_1005 (where X represents any amino acid residue). Directly upstream of Csal_1005, Csal_1004 encodes a predicted 428-amino-acid protein that shares amino acid sequence similarity with the catalytic α-subunits of some function-characterized Rieske nonheme iron oxygenases (ROs), such as the stachydrine demethylase (Stc2) (46% identity) from *Sinorhizobium meliloti* 1021 (24) and the oxygenase component of naphthalene 1,2-dioxygenase from *Pseudomonas* sp. strain NCIB 9816-4 (34%) (25). Conserved domain analysis revealed that Csal_1004 contains the conserved sequence CXHX$_{15-17}$CX$_2$H, which binds the Rieske-type [2Fe-2S] cluster at its

N-terminal region (Fig. 1C), and one nonheme Fe(II) domain, $(E/D)X_2HX_4H$, at its C-terminal region (Fig. 1C). Therefore, the Csal_1004-encoded protein might be a Rieske-type oxygenase. Based on the results of protein conserved domain analysis, we hypothesized that Csal_1004 and Csal_1005 potentially function as the terminal oxygenase component and the ferredoxin reductase component of the Rieske-type oxygenase system which is involved in the degradation of GB to dimethylglycine, and designated the *bmoA* and *bmoB* genes, respectively.

Targeted gene deletion and complementation assays. To verify the role of the *bmoA* and *bmoB* genes involved in the first step of GB degradation, the unmarked in-frame deletion mutants of *bmoA* (3043Δ*bmoA* mutant strain) and *bmoB* (3043Δ*bmoB* mutant strain) were constructed using the allelic exchange method. The wild-type *bmoA* gene was reduced to an open reading frame (ORF) of 39 nucleotides encoding only 12 amino acids (MDLLPSLHIVQG), while the wild-type *bmoB* gene was reduced to an ORF of 45 nucleotides encoding 14 amino acids (MTQNFFKSHVAIEF). *C. salexigens* DSM 3043, ZW4-1, 3043Δ*bmoA*, and 3043Δ*bmoB* were inoculated onto C-M63 agar plates supplemented with glucose, GB, or dimethylglycine at a final concentration of 20 mM as the sole carbon source to determine their GB- and dimethylglycine-degrading abilities. As predicted, strains 3043Δ*bmoA* and 3043Δ*bmoB* could utilize glucose or dimethylglycine as the sole carbon source but were incapable of growth on 20 mM GB as the sole source of carbon, while *C. salexigens* DSM 3043 and ZW4-1 could utilize glucose, GB, or dimethylglycine as the sole source of carbon (Fig. S2), indicating that the *bmoA* and *bmoB* genes are essential for the conversion of GB to dimethylglycine in *C. salexigens* DSM 3043.

To further determine whether the deficiency in GB-to-DMG conversion was due to inactivation of *bmoA* and *bmoB*, the *C. salexigens* 3043Δ*bmoA* and 3043Δ*bmoB* strains were complemented by their wild-type genes which were expressed under the control of their native promoters with a broad-host-range vector, pBBR1MCS. After the plasmids for complementation were conjugated into the mutant strains, strain 3043Δ*bmoA* carrying pBBR1MCS-bmoA and strain 3043Δ*bmoB* carrying pBBR1MCS-bmoB partially restored their abilities to use GB as the sole source of carbon in C-M63 medium (Fig. 2), while as the negative control, strains 3043Δ*bmoA* and 3043Δ*bmoB* carrying pBBR1MCS did not grow on the same medium (data not shown), confirming the role of these two genes in GB degradation to dimethylglycine. In addition, these results also implied that the *bmoA* and *bmoB* genes may utilize a common intergenic DNA sequence (286 bp) as their promoter regions in *C. salexigens* cells, although the two genes are predicted to be transcribed in opposite directions (Fig. S3). Interestingly, the 286-bp intergenic region (containing the *bmoB* promoter region) exhibited 41.35% sequence similarity with its reverse complement sequence (containing the *bmoA* promoter region) (Fig. S4). Compared manually with the known promoter sequences of *E. coli* or *C. salexigens ectA* (26), no conserved promoter sequence was detected. However, using the promoter prediction software NNPP version 2.2 (http://www.fruitfly.org/seq_tools/promoter.html) (27), a possible promoter region of Csal_1005 was detected, and its predicted transcription start site was located 45 bp upstream of the translation start codon (Fig. S4). To verify the actual promoter regions of Csal_1004 and Csal_1005, S1 nuclease mapping and primer extension experiments should be performed in future studies.

Functional characterization of BmoA and BmoB in *E. coli* cells. To check the proposed function of BmoA and BmoB, plasmid pACYC-bmoA-bmoB, which contained the *bmoA* and *bmoB* genes under the control of their respective T7 promoters in vector pACYCDuet-1, was transformed into *E. coli* BL21(DE3), while plasmids pACYC-bmoA, pACYC-bmoB, and pACYCDuet-1 were individually transformed into *E. coli* BL21(DE3) as the control. The transformed cells were grown in LB liquid medium, and protein expression was induced by isopropyl-β-D-thiogalactoside (IPTG). Since yeast extract in LB medium is known to contain 1 to 3% (wt/wt) GB (28), the GB transporters located on the cellular membrane of *E. coli* could transport them from growth media into the cells (29). As long as both *bmoA* and *bmoB* expression products are biologically active and
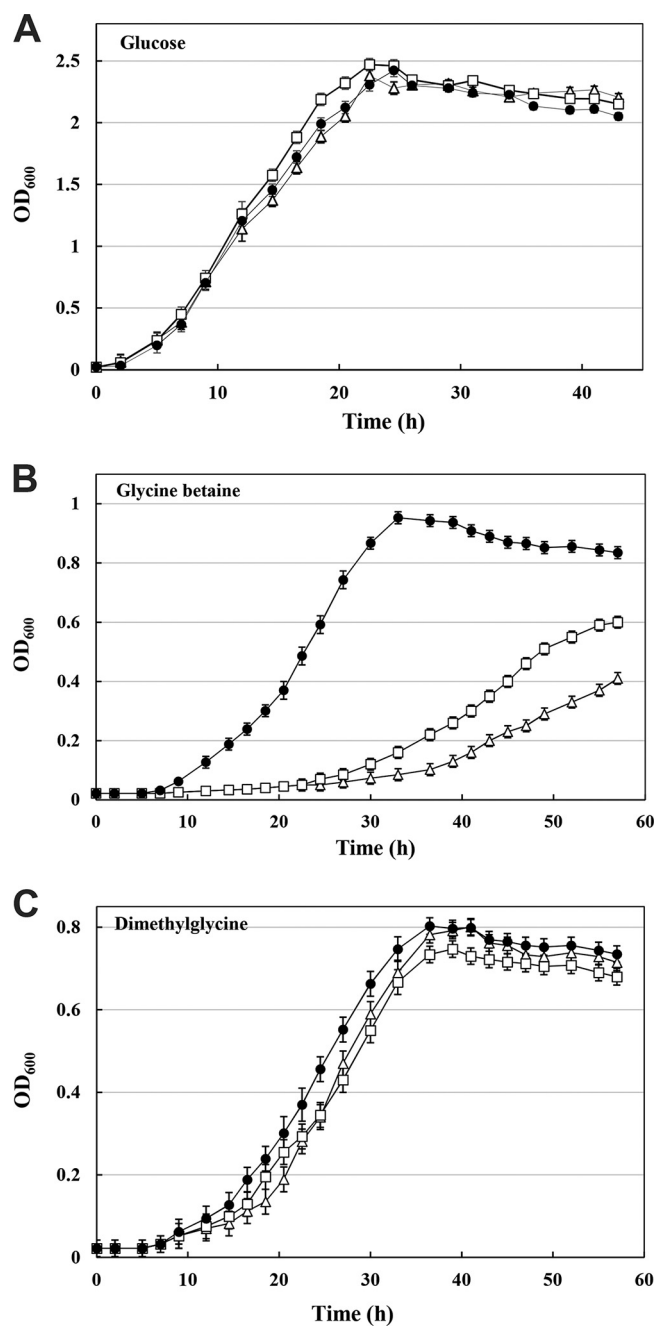
FIG 2 Growth of *C. salexigens* ZW4-1 (filled circle), 3043Δ*bmoA*(pBBR1MCS-bmoA) (open triangle), and 3043Δ*bmoB*(pBBR1MCS-bmoB) (open square) at 37°C in C-M63 liquid medium supplemented with glucose (A), GB (B), or dimethylglycine (C) as the sole source of carbon.

sufficient for bioconversion of GB to dimethylglycine, dimethylglycine will be detected intracellularly in *E. coli* cells. As shown in Fig. 3, ^{13}C nuclear magnetic resonance (NMR) analysis revealed that dimethylglycine was indeed accumulated in *E. coli* BL21(DE3) harboring pACYC-bmoA-bmoB, whereas GB was accumulated in *E. coli* BL21(DE3) harboring pACYC-bmoB or pACYCDuet-1. Unexpectedly, dimethylglycine was also found to accumulate in *E. coli* BL21(DE3) carrying plasmid pACYC-bmoA, which suggested that the cellular components in *E. coli* cells could substitute the function of the *bmoB*-encoded protein and convert GB to dimethylglycine in the presence of BmoA. This phenomenon has been observed in many multicomponent oxygenase systems (30), in which the flavin reductase components are usually nonspecific and interchange-
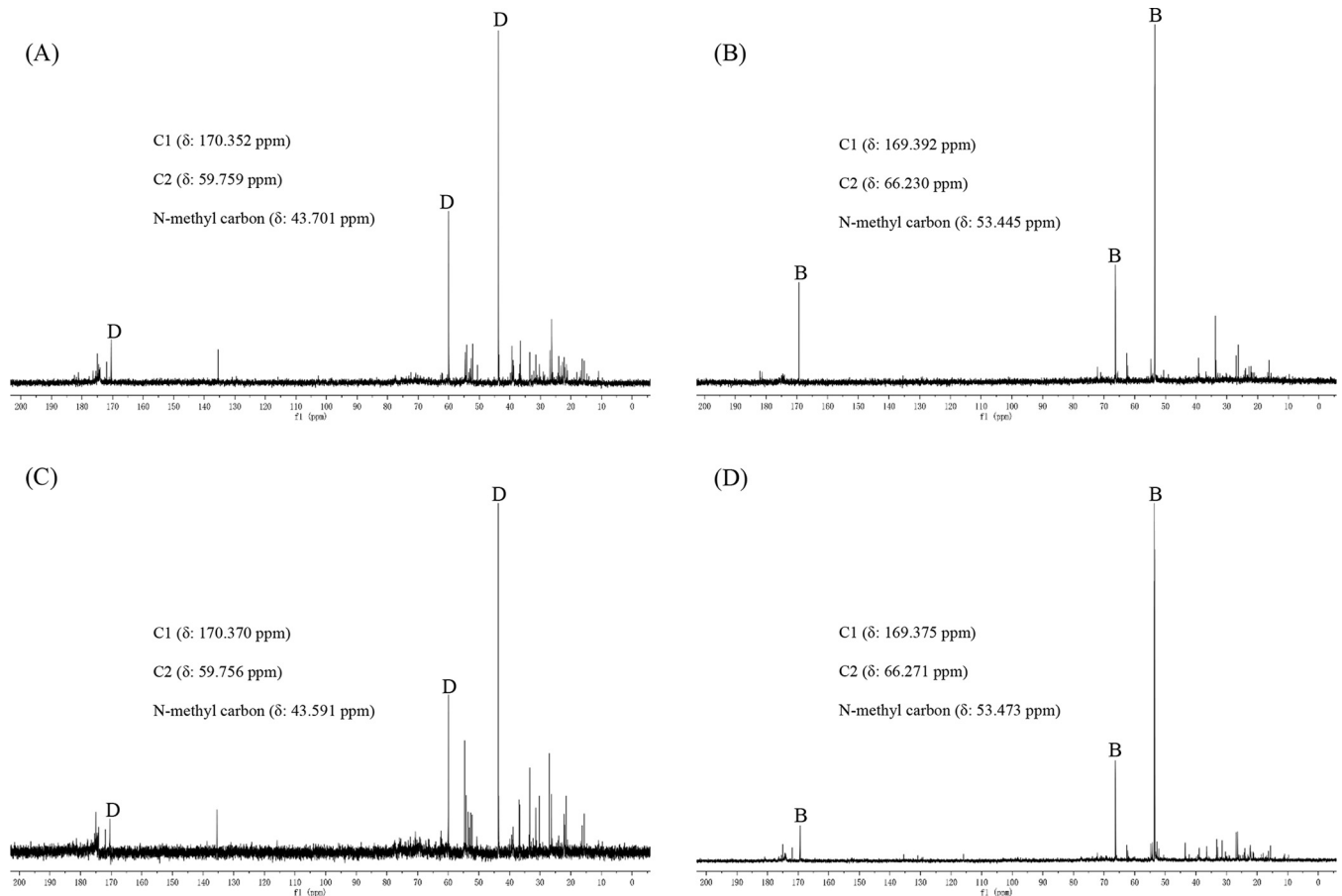
FIG 3 Natural-abundance ^{13}C NMR spectra of ethanolic extracts from *E. coli* BL21(DE3) cells harboring different recombinant plasmids grown in LB medium after induction with IPTG. Details for the induction of protein with IPTG and sample preparation are given in Materials and Methods. (A) *E. coli* BL21(DE3) harboring pACYC-bmoA. (B) *E. coli* BL21(DE3) harboring pACYC-bmoB. (C) *E. coli* BL21(DE3) harboring pACYC-bmoA-bmoB. (D) *E. coli* BL21(DE3) harboring pACYCDuet-1. B, glycine betaine; D, dimethylglycine.

able and can be substituted by the flavin reductases from other bacteria, such as SsuE, the flavin reductase component of alkanesulfonate monooxygenase from *E. coli* (31). The possibility that the SsuE or other uncharacterized ferredoxin reductases in *E. coli* replace the function of BmoB may well explain why *E. coli* BL1(DE3) carrying the *bmoA* gene in the absence of the *bmoB* gene was still capable of degrading GB to dimethylglycine. In addition, to test whether the promoter regions of *bmoA* and *bmoB* could be recognized by *E. coli* transcriptional system, plasmid pBBR1MCS-bmoA-bmoB, which contained the full-length *bmoA* and *bmoB* genes, and their intergenic sequence was introduced into competent *E. coli* BL21(DE3) or *E. coli* DH5α cells. ^{13}C NMR analysis indicated that GB, but not dimethylglycine, was accumulated in *E. coli* (data not shown). The failure of *E. coli* BL21(DE3) or DH5α carrying pBBR1MCS-bmoA-bmoB to decompose GB to dimethylglycine may due to many possible reasons, including a lack of recognition of *C. salexigens* promoter regions by *E. coli* RNA polymerases or a lack of the necessary transcriptional regulatory factor to activate gene transcription in *E. coli*.

Purification of His$_6$-tagged BmoA and BmoB. To characterize the biochemical properties of BmoA and BmoB, we individually overexpressed them using the pET28a(+) expression system in *E. coli* BL21(DE3) as C-terminal and N-terminal His$_6$-tagged fusion proteins to facilitate protein purification. We found that the fusion protein with a His$_6$ tag at the N terminus of BmoA (His$_6$-BmoA) was expressed as inclusion bodies and did not show activity, although many attempts, including reducing the incubation temperature and the concentration of inducer, or replacing the expression host and vector to enhance the yield as the soluble form, were made. Fortunately, this situation had
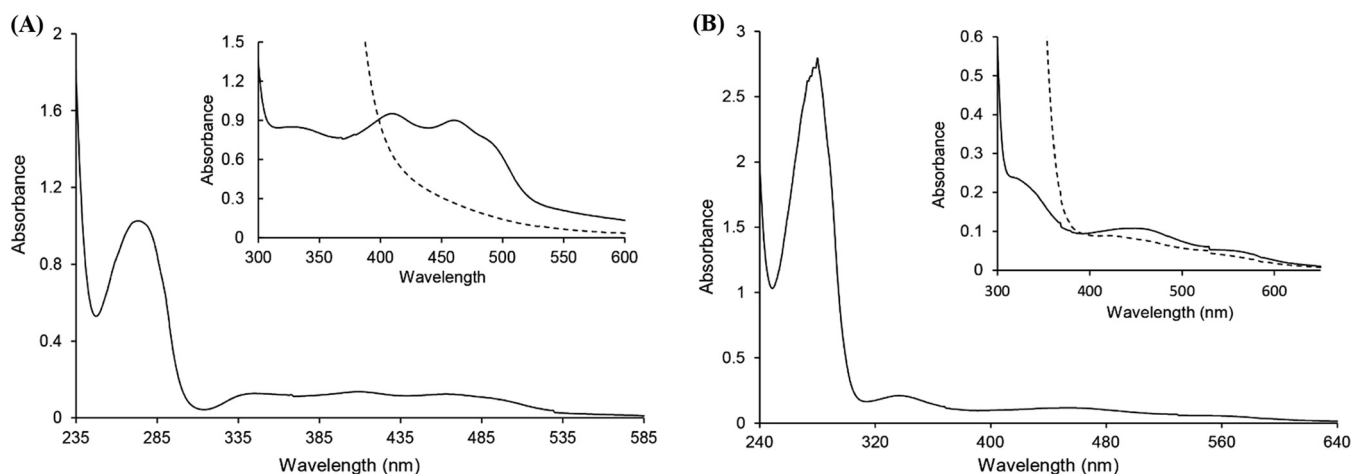
FIG 4 UV-visible absorption spectra of the purified His$_6$-BmoB (19.09 μM) (A) and BmoA-His$_6$ (22.84 μM) (B) in 50 mM Tris-HCl (pH 7.0). (A) The inset shows the magnified absorption spectra of the purified His$_6$-BmoB (0.14 mM protein) before (solid line) and after (dashed line) the addition of sodium dithionite (2 mM). (B) The inset shows the magnified absorption spectra of BmoA-His$_6$ before (solid line) and after (dashed line) the addition of sodium dithionite (2 mM).

been greatly improved when the His$_6$ tag was switched from the N terminus to the C terminus of the BmoA (BmoA-His$_6$) (Fig. S5A), and the BmoA-His$_6$ was predominantly expressed as the soluble form in *E. coli*. On the other hand, the recombinant protein with a His$_6$ tag added at the N terminus of the BmoB (His$_6$-BmoB) (Fig. S5A) was found in the supernatant and sediment of *E. coli* cell lysate. As estimated from SDS-PAGE, BmoA-His$_6$ and His$_6$-BmoB represented roughly 20 to 40% of the total protein in the cell extracts. After being individually purified to electrophoretic homogeneity using a nickel dication-nitrilotriacetic acid (Ni^{2+}-NTA)-chelating column, the yields of purified BmoA-His$_6$ and His$_6$-BmoB were estimated to be about 22.6 $\pm$ 3.5 mg and 13.8 $\pm$ 2.5 mg per liter of culture. The enzyme preparations of His$_6$-BmoB were stable for at least 2 weeks when stored at -40°C in elution buffer with no addition of enzyme stabilizer, whereas the BmoA-His$_6$ solution was very unstable and only maintained no more than 10% residual activity after the same treatment. Although we tried to add the protective agents, such as glycerol, to the BmoA enzyme preparation, the protective effect was still very limited.

Molecular weights and subunit composition. SDS-PAGE analysis revealed the presence of only one protein band for purified BmoA-His$_6$ or His$_6$-BmoB, and their molecular masses were determined to be approximately 52.5 kDa and 47.7 kDa, respectively, in agreement with the predicted size of the proteins. The native molecular masses of purified BmoA-His$_6$ and His$_6$-BmoB were estimated by gel filtration to be 154.8 and 45.1 kDa, respectively (Fig. S5B), suggesting a homotrimeric structure (α3) for BmoA and a monomeric structure for BmoB.

Biochemical characterization of BmoB as an NAD(P)H-dependent flavin reductase. (i) Spectroscopic properties. The purified His$_6$-BmoB preparation was bright yellow in color. The UV-visible spectra of the enzyme showed absorption maxima at 275, 325, 410, and 460 nm, with a shoulder at about 492 nm (Fig. 4A), which are typical of a flavoprotein (32). After the addition of sodium dithionite, the absorption peaks in the visible range disappeared, indicating the reduction of enzyme-bound flavin. The flavin prosthetic group is readily dissociated from BmoB by treatment with 5% trichloroacetic acid, suggesting it is uncovalently bound. After the flavin was extracted by boiling, high-performance liquid chromatography (HPLC) analysis identified it as FAD (Fig. 5). The molar ratio of FAD to protein was determined to be 0.66 $\pm$ 0.08, indicating that each BmoB contains one FAD molecule. It is likely that BmoB has lost part of its flavin during the purification process. Based on a molecular mass of 43.26 kDa, the contents of iron and acid-labile sulfide in the purified enzyme were determined to be 1.88 $\pm$ 0.05 mol and 1.76 $\pm$ 0.10 mol per mol His$_6$-BmoB, respectively, in agreement
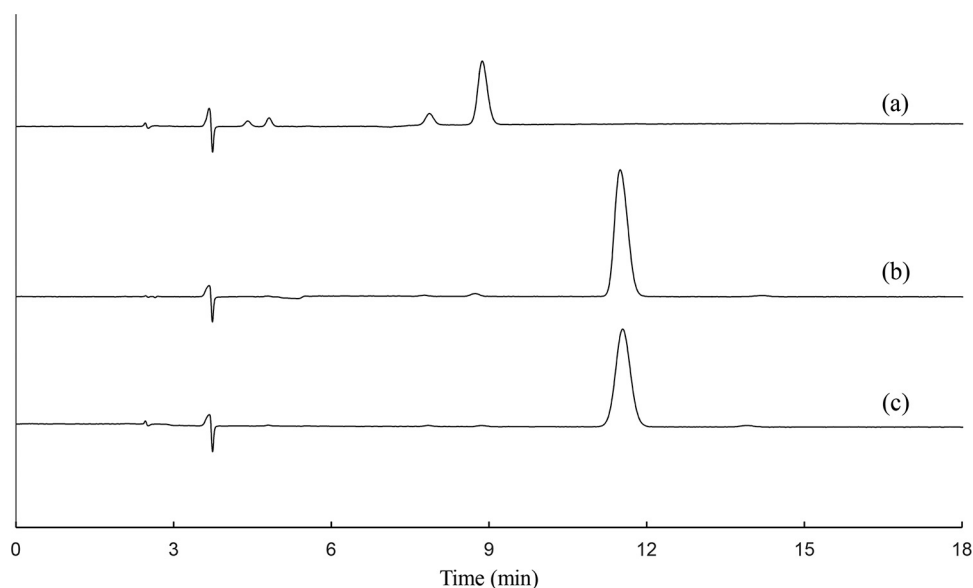
FIG 5 HPLC elution profiles identifying FAD as the flavin cofactor of His$_6$-BmoB. (a) Authentic FMN. (b) Sample of flavin cofactor extracted from BmoB by heat treatment. (c) Authentic FAD.

with the presence of a properly assembled [2Fe-2S] center in His$_6$-BmoB. These observations suggest that the native His$_6$-BmoB contains one [2Fe-2S] center and one FAD per enzyme.

(ii) Catalytic properties. The flavin reductase activity of BmoB could only be measured after the enzyme had been purified, since it is impossible to measure the crude enzyme activity due to the existence of high background NADH oxidation activity even with that of the negative-control *E. coli* BL21(DE3) harboring pET28a. BmoB could not only utilize NADH to reduce flavin mononucleotide (FMN), FAD, or riboflavin but also oxidize NADPH as the substrate, concomitantly producing hydrogen peroxide. The kinetic parameters of His$_6$-BmoB were determined (Table 1), and NADH appeared to be the preferred electron donor over NADPH, while FMN was the most favored electron acceptor for BmoB compared with FAD and riboflavin. Interestingly, although FAD was found to be the native cofactor for BmoB, the oxidation rate for NADH in the presence of FMN was slightly higher than that in the presence of FAD. The addition of GB to the reaction mixtures did not result in any changes toward His$_6$-BmoB activity on its substrates, and no formaldehyde or dimethylglycine was detected without BmoA-His$_6$. The optimal pH was determined to be 7.5 in Tris-HCl buffer, with 47, 82, 85, and 62% of the activity maintained at pH 6.5, 7.0, 8.0, and 8.5, respectively. From the results obtained, it can be concluded that BmoB is an NAD(P)H-dependent flavin reductase.

Biochemical characterization of BmoA as a Rieske-type oxygenase. (i) Spectroscopic properties. The purified BmoA-His$_6$ preparation was red-brown in color, and the

TABLE 1 Apparent kinetic parameters for the reductase activity of His$_6$-BmoB[a]

Substrate (concn range [μM]	V_{max} (μmol $\cdot$ mg^{-1} $\cdot$ min^{-1})	K_m (μM)	k_{cat} (s^{-1})	Cosubstrate
NADH (12.5–200)[b]	1.25 ± 0.07	43.94 ± 1.4	0.90 ± 0.01	FAD
NADPH (12.5–800)[b]	0.49 ± 0.05	257.80 ± 2.6	0.35 ± 0.01	FAD
FAD (2.5–200)[c]	5.90 ± 0.18	6.03 ± 0.13	4.25 ± 0.01	NADH
FMN (2.5–200)[c]	6.79 ± 0.12	17.31 ± 0.11	4.89 ± 0.01	NADH
Riboflavin (2.5–500)[c]	2.32 ± 0.15	111.83 ± 6.75	1.67 ± 0.01	NADH

[a]Experiments were performed in 50 mM Tris-HCl (pH 7.0) at 25°C. Values are means of and standard deviations of the results from three independent sets of experiments.
[b]Determined with a fixed FAD concentration of 150 μM.
[c]Determined with a fixed NADH concentration of 200 μM.

air-oxidized enzyme had absorption maxima at 279, 326, and 460 nm, with a shoulder at about 572 nm (Fig. 4B), a typical characteristic and similar to the proteins containing a Rieske-type [2Fe-2S] center (33, 34). In fact, the entire absorbance spectrum of BmoA was almost the same as those of the choline monooxygenase (CMO) from *Spinacia oleracea* (35) and the terminal oxygenase (OxoO) of 2-oxo-1,2-dihydroquinoline 8-monooxygenase from *P. putida* 86 (32), which contain both a [2Fe-2S] cluster and mononuclear nonheme iron in a 1:1 ratio. After the addition of 2 mM sodium dithionite, the absorption peak at 460 nm decreased by about 29%, while two new absorption peaks appeared at 418 nm and 521 nm (Fig. 4B, inset). When the concentration of sodium dithionite was increased to 8 mM, the color of enzyme solution faded, and the absorption in the visible region disappeared, a phenomenon commonly observed in iron-sulfur proteins (35). The iron and acid-labile sulfide contents of BmoA-His$_6$ were estimated to be 2.59 $\pm$ 0.12 and 1.93 $\pm$ 0.08 mol per mol enzyme monomer. After the addition of FeSO$_4$ (1 mM) to the purified BmoA-His$_6$, the enzyme solution was desalted with Sephadex G25 (Sigma). The iron content of purified BmoA-His$_6$ increased to 3.09 $\pm$ 0.06 mol per mol enzyme monomer, indicating the corresponding subunit of iron-sulfur proteins contains one [2Fe-2S] cluster and one nonheme iron. Based on these data, it could be expected that the native BmoA-His$_6$, as a homotrimer, contains a [2Fe-2S] center and mononuclear iron per subunit.

(ii) **Catalytic properties.** The BMO activity of BmoA was measured by monitoring GB-dependent formaldehyde production in the presence of BmoB. Dimethylglycine and formaldehyde were absent if heat-denatured BmoA was used or if GB was omitted from the enzyme assay, which indicated that dimethylglycine and formaldehyde were derived enzymatically from GB. In the absence of BmoB, BmoA showed no detectable BMO activity. The observation that BmoA activity was absolutely dependent on the presence of BmoB supports our hypothesis that both components are required and sufficient for the conversion of GB to dimethylglycine. Although BmoB could use NADH or NADPH as the electron donors with different efficiencies, the activity of BmoA was strictly dependent on NADH, and GB degradation was negligible when NADPH was used instead of NADH, revealing the NADH-dependent GB monooxygenase activity. Maximal activity was obtained when the reaction mixtures were vigorously stirred on a magnetic stirrer. Under anaerobic conditions, no formaldehyde or dimethylglycine could be detected. However, after the anaerobic reaction mixtures were exposed to air, formaldehyde and dimethylglycine were detected in the reaction mixtures, indicating that the GB demethylation reaction was absolutely dependent on the presence of oxygen. The optimal pH and temperature for the enzyme were 7.5 and 30°C, respectively. With 5 mM NADH and 5 μM FAD as the cofactor, the apparent K_m and k_{cat} values of BmoA for GB were determined to be 1.20 $\pm$ 0.01 mM and 0.65 $\pm$ 0.10$_s$$^{-1}$, respectively. BmoA could use all three kinds of flavins as cofactors, and the specific activities of BmoA with FAD, FMN, and riboflavin as the cofactor were determined to be 11.64, 13.89, and 6.56 U/mg, respectively. The stoichiometry data showed that GB consumption was accompanied by the formation of equimolar amounts of dimethylglycine and formaldehyde under aerobic conditions.

(iii) **Substrate specificity.** The substrate range of BmoA was investigated *in vitro* by measuring the formation of formaldehyde spectrophotometrically (Fig. S6) and detecting the potential substrate demethylation products with ^{13}C NMR spectroscopy (Fig. S7). The results indicated that BmoA could specifically utilize GB as substrate, and did not show any activity on choline, L-carnitine, stachydrine, dimethylglycine, or sarcosine.

Effects of the molar ratios of BmoA to BmoB on BMO activity. Since the BMO activity of BmoA was dependent on the presence of BmoB, the influence of molar ratio of BmoA to BmoB on BMO activity was investigated. As shown in Fig. 6, maximal specific activity was obtained when the ratio of BmoA to BmoB was 5:1, with FAD as the cofactor *in vitro* assays, indicating that the demethylation activity of BmoA was highly dependent on the molar ratio of BmoA to BmoB. Thus, the ratio of 5:1 was employed throughout the *in vitro* BMO activity assays.
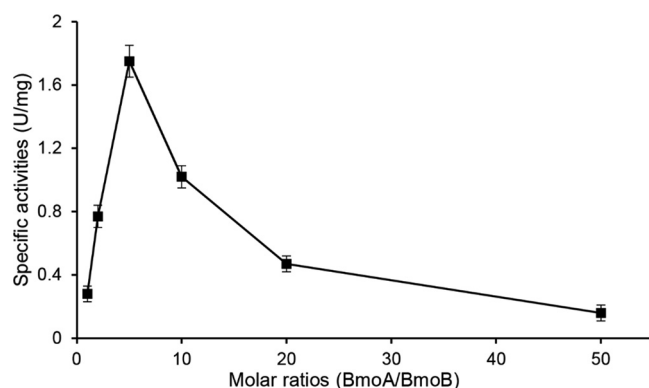
FIG 6 Effects of the molar ratios of BmoA to BmoB on BMO activity. The specific activities were measured by the amount of formaldehyde produced after shaking at 30°C for 30 min while keeping the concentration of BmoB constant at 1.5 μM and varying the concentration of BmoA (1.5 to 75 μM) in the reaction mixture containing 10 μM FAD, 5 mM NADH, and 2 mM GB.

Effects of flavin concentrations on BMO activity. During the process of optimizing the concentrations of each component in the reaction mixture, we found that higher concentrations of flavins ($>$15 μM for FAD and $>$25 μM for FMN) would lead to a decrease in BmoA-specific activity but have no inhibitory effect on the flavin reductase activity of BmoB (data not shown). Inhibition by high flavin concentrations was also observed in the p-hydroxyphenylacetate hydroxylase from *Acinetobacter baumannii* (36) and the luciferase from *Vibrio harveyi* (37). It was believed that the excess oxidized flavin competed with the reduced flavin for the flavin-binding sites on the reductase, leading to the decline in electron transfer efficiency (36).

Effects of metal ions and EDTA on BMO activity. As shown in Table 2, the BMO activity was significantly enhanced by Fe^{2+} and severely inhibited by heavy-metal ions, including Co^{2+}, Mn^{2+}, Zn^{2+}, Cu^{2+}, and Ag^+. The presence of K^+, Na^+, or Mg^{2+} has no obvious influence on it activity, while the addition of Ca^{2+} resulted in 21% inhibition of activity. It should be noted that addition of the metal chelating-agent EDTA severely inhibited BMO activity, suggesting that the enzyme needs metal ions for its activity.

DISCUSSION

In this study, a novel RO system, GB monooxygenase (BMO), was identified and molecularly characterized. This system is composed of a Rieske-type oxygenase component (BmoA) and a NADH-dependent flavin reductase component (BmoB), and it catalyzes the oxidative N-demethylation of GB to dimethylglycine in *C. salexigens* DSM 3043. In terms of GB degradation products, the oxidation mechanism of BMO toward

TABLE 2 Effects of metal ions and EDTA on BMO activity

Chemical agent or metal ion[a]	Relative activity (%)
Control (no ions added)	100[b]
Na$^+$	98 $\pm$ 2
K$^+$	99 $\pm$ 2
Ag$^+$	ND[c]
Fe^{2+}	260 $\pm$ 15
Mg^{2+}	96 $\pm$ 1
Cu^{2+}	DN[d]
Co^{2+}	34 $\pm$ 2
Ca^{2+}	79 $\pm$ 3
Zn^{2+}	DN[d]
Mn^{2+}	ND[c]
EDTA	11 $\pm$ 2

[a]The final concentration of tested ions was 2 mM.
[b]The activity of 4.29 U/mg was set as 100%.
[c]ND, not detectable.
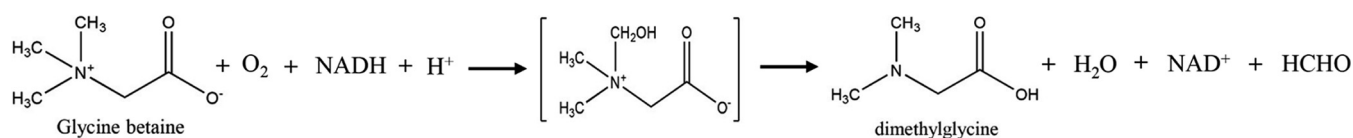[d]DN, the enzyme was denatured after the addition of ions.

FIG 7 Proposed reaction mechanism for BMO-catalyzed conversion of GB to dimethylglycine in *C. salexigens* DSM 3043. A hypothetical intermediate (brackets) spontaneously decomposes in formaldehyde and dimethylglycine.

GB, similar to those of 4-methoxybenzoate monooxygenase (38) and dicamba monooxygenases (39), was proposed (Fig. 7). BMO catalyzes oxygen attack at a methyl group in GB, rather than the oxygenation of the aromatic ring that was observed in most other Rieske nonheme iron ring-hydroxylating oxygenases (RHOs), and it inserts an oxygen atom into the methyl C—H bond. The *N*-methyl group in GB is then oxidized to an *N*-methylol intermediate, and the intermediate would likely decompose spontaneously, releasing dimethylglycine and formaldehyde. Another possibility, that the activated oxygen species attacks the methyl group in a nucleophilic substitution-type reaction, can be excluded, since the reaction product would be methanol rather than formaldehyde in that case. Because the *in vivo* experiment indicated that dimethylglycine-was accumulated in *E. coli* expressing BmoAB or BmoA, it can be confirmed that the predicted catabolism does occur in bacterial cytosol. On the other hand, formaldehyde, the second product of catalysis, is toxic to cells. It can either be assimilated into cell biomass via the various formaldehyde assimilation pathways or dissimilated via formate to carbon dioxide by the action of formaldehyde dehydrogenases and formate dehydrogenases, generating the reducing equivalents for energy generation and biosynthesis. BLAST searches of the *C. salexigens* DSM 3043 genome revealed in the vicinity of *bmoA* and *bmoB* genes and other locations in the genome, several putative ORFs may encode predicted glutathione-independent formaldehyde dehydrogenases (Csal_0335 and Csal_0995) and formate dehydrogenases (Csal_0997, Csal_1915, and Csal_1917).

It is well known that prokaryotic RO systems are made up of two or three components. Most of these component-encoding genes are usually located on different loci that separated them for at least several kilobases (40, 41), while other genes are organized in one operon and transcribed in the same direction. However, this is not the case for the BMO-encoding genes (*bmoA* and *bmoB*) from *C. salexigens* DSM 3043. Although the two genes are found adjacent to each other, they are transcribed in divergent directions, which is an interesting gene arrangement that has rarely occurred in the function characterized RO systems. We believed that this arrangement increases the flexibility of the cells to cope with environmental changes, since the transcription of *bmoB* might be controlled not only by the intracellular concentration of GB but also by other environmental factors.

Among the biochemical characterized ROs, BmoA showed the highest sequence homology (46% similarity) to the stachydrine demethylase Stc2 from *S. meliloti* 1021 (42), while BmoB exhibited the highest sequence homology (27% similarity) to the reductase component of the benzoate dioxygenase from *Acinetobacter* sp. strain ADP1 (43). The low amino acid sequence similarities suggest that BMO is a novel two-component Rieske-type monooxygenase system.

According to the classification system made by Batie et al. (44), multicomponent RHOs were classified into three main classes (classes I, II, and III) in terms of the number of protein components and the nature of their redox centers involved in electron transport from NAD(P)H to the oxygenase component. Class I RHOs, as the two-component oxygenase system, were further subdivided into subclass A and subclass B based on the cofactor (FMN/FAD) binding to the reductase component. Since biochemical characterization of BmoB showed the presence of FAD as the native cofactor, and an *in vitro* assay proved that BMO contains two components (BmoA and BmoB), BMO should belong to the class IB Rieske-type oxygenase. However, the FAD binding motif is found at the N terminus of BmoB and does not locate between the [2Fe-2S] binding
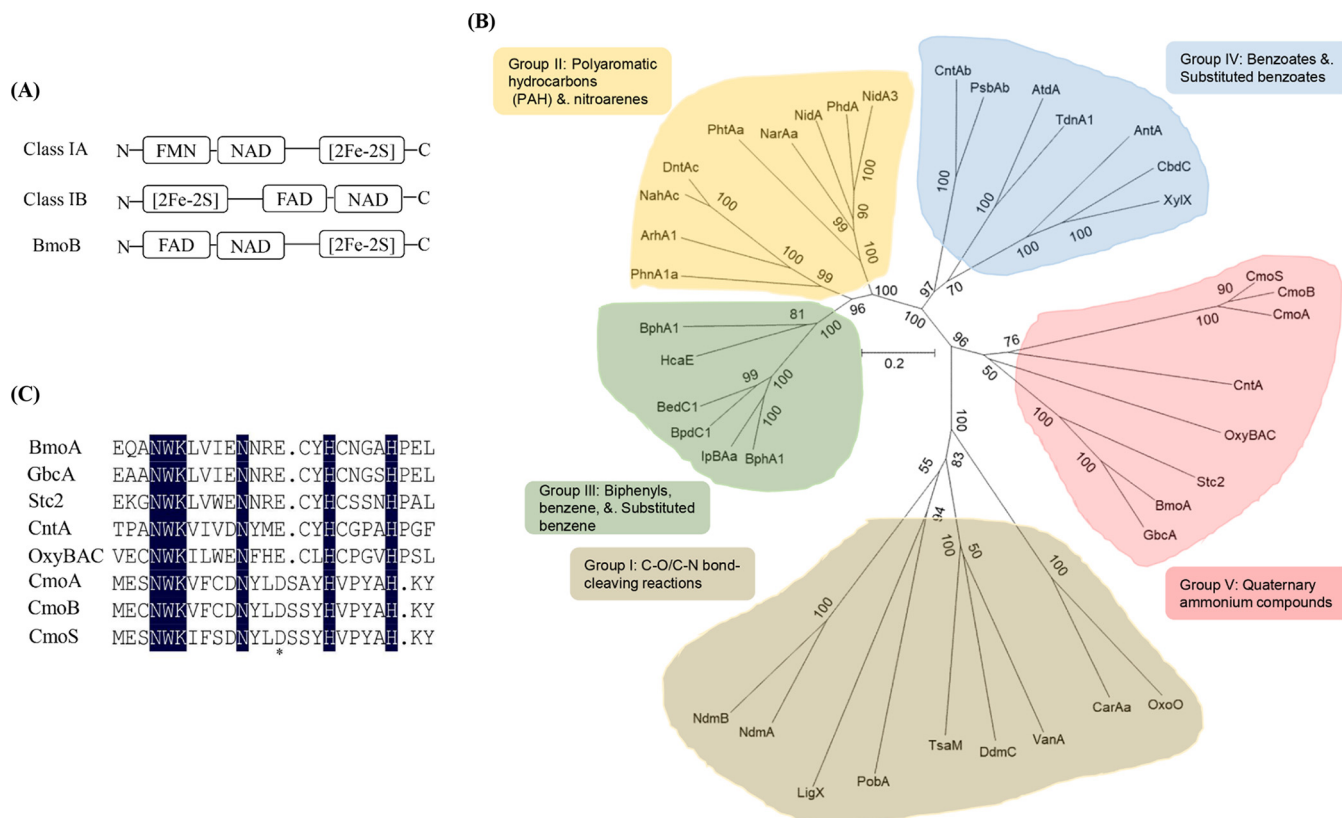
FIG 8 Identification of the putative Rieske-type protein involved in GB-to-dimethylglycine degradation from *C. salexigens* DSM 3043. (A) Organization of the cofactor binding domains in class IA, class IB, and BmoB. (B) Classification of the large subunits of 39 terminal oxygenase components in Rieske nonheme iron oxygenases. The phylogenetic tree, inferred by the neighbor-joining method, shows the relative positions of BmoA among other characterized ROs based on the Nam classification system (42). Bootstrap values for 1,000 replications are given. The scale bar represents two substitutions per 10 amino acids. The protein abbreviations, their corresponding species, and gi/accession numbers in the GenBank database are as follows: OxoO, *P. putida* 86, 2072732; CarAa, *Pseudomonas* sp. strain CA10, 2317678; VanA, *Pseudomonas* sp. HR199, 1946284; DdmC, *Pseudomonas maltophilia* DI-6, 55584974; TsaM, *Comamonas testosteroni* T-2, 1790867; PobA, *P. pseudoalcaligenes* POB310, 473250; LigX, *Sphingomonas paucimobilis* SYK-6, 4062861; NdmA, *P. putida* CBB5, AFD03116; NdmB, *P. putida* CBB5, AFD03117; BphA1, *P. pseudoalcaligenes* KF707, 151091; IpBAa, *P. putida* RE204, 2822265; BpdC1, *Rhodococcus* sp. strain M5, 927232; BedC1, *P. putida* ML2, 1168640; HcaE, *E. coli* K-12, 81170783; BphA1, *Rhodococcus erythropolis* TA421, 3059209; PhnA1a, *Sphingomonas* sp. strain CHY-1, 75455648; ArhA1, *Sphingomonas* sp. strain A4, 50725019; NahAc, *Pseudomonas* sp. strain JS42, 1224114; DntAc, *Burkholderia cepacia* R34, 17942397; PhtAa, *Mycobacterium vanbaalenii* PYR-1, 49072886; NarAa, *Rhodococcus* sp. strain NCIMB12038, 4704462; NidA, *M. vanbaalenii* PYR-1, 11038552; PhdA, *Nocardioides* sp. strain KP7, 7619816; NidA3, *M. vanbaalenii* PYR-1, 68053509; CntAb, *P. putida* F1, 1263180; PsbAb, *Rhodopseudomonas palustris*, 5360700; AtdA, *Acinetobacter* sp. strain YAA, 1395141; TdnA1, *P. putida* UCC22, 1841362; AntA, *Acinetobacter* sp. ADP1, 3511232; CbdC, *Burkholderia cepacia* 2CBS, 758210; XylX, *P. putida* TOL, 139861; CmoS, *Spinacia oleracea*, AAB52509; CmoB, *Beta vulgaris*, AAB80954; CmoA, *Amaranthus tricolor*, AAK82768; CntA, *A. baumannii* ATCC 19606, EEX03955; OxyBAC, *Pseudomonas* sp. BIOMIG1, 1057213843; Stc2, *S. meliloti* 1021, 16262853; BmoA, *C. salexigens* DSM 3043, 759867680; and GbcA, *P. aeruginosa* PAO1, 15600603. (C) Multiple-sequence alignment of BmoA and the members in group V of the RO family. The asterisk (*) indicates the conserved glutamate residue in the mononuclear iron center domain of microbial RO oxygenase component, while identical amino acids residues in the eight sequences are shown in black.

domain and the NAD binding domain, suggesting that BMO does not belong to any of these classes (Fig. 8A). Carnitine oxygenase, a recently identified RO from *A. baumannii* ATCC 19606, has a similar modular arrangement (45).

Although most of microbial ROs reported normally catalyze the initial oxygenation reaction of various aromatic compounds, more recently discovered ROs have been found to be capable of catalyzing non-ring-hydroxylating reactions (24, 45, 46). Studies on protein crystal structure revealed that the large subunit (α-subunit) of terminal oxygenase component in the oxygenase system is responsible for determining the substrate specificity of the enzyme (47). Although the terminal oxygenase components in RO systems share a conserved domain structure, their sequences are highly divergent (48). To gain insight into the evolutionary relationship between the BmoA and other characterized ROs, phylogenetic analysis of BmoA was conducted with the large subunits of 38 representative ROs. All of these ROs are divided into five groups (Fig. 8B), and BmoA is clustered into RO group V, a novel group established by Ertekin et al. (46), according to the nomenclature system of Nam et al. (49), who proposed another

classification scheme based on the homology of the amino acid sequences of the large subunits of the terminal oxygenase components, and classified them into 4 groups (groups I to IV) according to substrate preferences. The members in the RO group V include the CntA of carnitine oxygenase from *A. baumannii* ATCC 19606 (45), the Stc2 (stachydrine demethylase) from *S. meliloti* 1021 (42), the GbcA as the predicted GB dioxygenase from *P. aeruginosa* PAO1 (19), the OxyBAC (benzalkonium chloride oxygenase) from *Pseudomonas* sp. strain BIOMIG1 (46), and three choline monooxygenases from plants (Fig. 8B). A common feature of these enzymes is that they could use quaternary ammonium compounds (QACs) as substrates and initiate the first step of QAC degradation through *N*-dealkylation reactions, attacking the $C-N^+$ bond between the methyl group and quaternary N in QACs to remove the methyl group from the N atom.

Further analysis of the catalytic mononuclear iron centers in this newly established group revealed that all the terminal components of microbial ROs have the conserved glutamate residue instead of the conserved aspartate residue found in the other groups of ROs (Fig. 8C). The conserved glutamate is considered to be essential in intermolecular electron transfer from the Rieske center of one monomer to the active nonheme mononuclear iron site in the neighboring monomer (45, 50). The substitution of the original aspartate residue with glutamate in naphthalene dioxygenase (51) or glutamate with an aspartate residue in carnitine oxygenase resulted in a severe loss of enzyme activity (45). Interestingly, the same sites in the choline monooxygenases from plants in the RO group V were the conserved aspartate residue (Fig. 8C), the same as those ROs in the other groups. The roles of this residue in BmoA and other eukaryotic choline monooxygenases remain to be investigated in prospective work.

MATERIALS AND METHODS

Chemicals. GB, dimethylglycine, sarcosine, flavin mononucleotide (FMN), flavin adenine dinucleotide (FAD), riboflavin, NADH, and NADPH were purchased from Sigma-Aldrich Chem (Shanghai, China). Nickel-nitrilotriacetic acid (Ni-NTA) Sefinose resin, choline, carnitine, hydrogen peroxide, and isopropyl-β-D-thiogalactoside (IPTG) were purchased from Sangon Biotech (Shanghai, China). Stachydrine was purchased from Aladdin Bio-Chem Tech (Shanghai, China). Restriction enzymes, T4 DNA ligase, and *Taq* DNA polymerase were purchased from TaKaRa Biotech (Dalian, China) and used according to the manufacturer's procedures. All other chemical reagents used in this study were of analytical grade and are commercially available.

Bacterial strains, plasmids, and growth conditions. The bacterial strains and plasmids used in this study are listed in Table 3, and the primers are shown in Table 4. *C. salexigens* DSM 3043 and its mutants were routinely grown at 37°C in D5 medium (per liter, 50 g NaCl, 5 g $MgSO_4 \cdot 7H_2O$, 5 g tryptone, and 3 g yeast extract [pH 7.5]) or in C-M63 medium [per liter, 50 g NaCl, 2 g $(NH_4)_2SO_4$, 13.6 g KH_2PO_4, 3.6 g D-glucose, 0.12 g $MgSO_4$, and 0.5 mg $FeSO_4 \cdot 7H_2O$ (pH 7.5)]. *E. coli* strains were aerobically cultivated in Luria-Bertani (LB) medium (52) with shaking at 37°C and 180 rpm. For culture cells carrying an antibiotic resistance marker, antibiotics were added at the following concentrations: 50 $\mu g \cdot ml^{-1}$ rifampin (Rif), 70 $\mu g \cdot ml^{-1}$ chloramphenicol (Cm), and 50 $\mu g \cdot ml^{-1}$ kanamycin (Km). The concentrations of GB, dimethylglycine, or glucose were 20 mM when used as the sole carbon source in the defined media. Cell growth was monitored by measuring the optical density at 600 nm (OD_{600}) with a UV2301II UV-visible spectrophotometer (Techcomp, Shanghai, China).

General DNA manipulations. Total genomic DNA from *C. salexigens* and *E. coli* strains was prepared with the Ezup column bacteria genomic DNA extraction kit (Sangon, China), while plasmid DNA was isolated using the SanPrep column plasmid mini-preps kit (Sangon). All PCR amplifications were performed using the *Pfu* PCR MasterMix (TianGen, China), and the amplified DNA fragments were purified using the SanPrep column DNA gel extraction kit (Sangon). Colony PCR was performed as described previously (23).

Inactivation of *bmoA* (csal_1004) and *bmoB* (csal_1005). The *bmoA* (Csal_1004) and *bmoB* (Csal_1005) single-gene in-frame deletion mutants of *C. salexigens* ZW4-1 were constructed by the allelic exchange method, as described previously (23). Briefly, the upstream and downstream regions of the target gene were PCR amplified from the genome of strain ZW4-1 (rifampin resistant [Rif^r]) with the primer pairs listed in Table 4, fused together by splicing by overlapping extension PCR (SOE-PCR) (53), and cloned into the double-restriction enzyme-digested plasmid pK18mobsacB (kanamycin resistant [Km^r]) (54), which is nonreplicative in *C. salexigens*. The resultant plasmid pK18mobsacB::ΔbmoA, containing the mutant allele of *bmoA* with an internal 1,248-bp deletion, or pK18mobsacB::ΔbmoB, containing the mutant allele of *bmoB* with an internal 1,062-bp deletion, was first transformed into *E. coli* S17-1 competent cells and then mobilized into *C. salexigens* ZW4-1 (Rif^r) via biparental mating. Single-crossover mutants were selected for growth on D5 plates with Rif and Km and verified by PCR with primers (sacB-F/sacB-R) to detect the backbone of the suicide vector. Double-crossover mutants were selected by growth on sucrose-containing D5 plates and verified by colony PCR with two primer sets

TABLE 3 Bacterial strains and plasmids used in this study

Strain or plasmid	Genotype or description[a]	Source or reference
Strains		
Chromohalobacter salexigens		
DSM 3043	Wild type	DSMZ[b]
ZW4-1	Spontaneous rifampin-resistant mutant of *C. salexigens* DSM 3043	23
3043Δ*bmoA*	*bmoA* in-frame deletion mutant of strain ZW4-1, Rif[r]	This study
3043Δ*bmoB*	*bdmB* in-frame deletion mutant of strain ZW4-1, Rif[r]	This study
E. coli		
DH5α	*supE44* Δ*lacU169* (Φ801*acZ*ΔM15) *hsdR17 recA1 endA1 gyrA96 thi-1 relA1*	TaKaRa
S17-1	*pro hsdR recA* [(RP4-2 (Tc::Mu)(Km::Tn7))]	23
BL21(DE3)	F⁻ *ompT hsdS*$_B$(r$_B$⁻ m$_B$⁻) *gal dcm* (DE3); T7 RNA polymerase gene under the control of the *lacUV* promoter	TianGen
Plasmids		
pK18mobsacB	*mob sacB* (RP4) *lacZ*, Km[r]	54
pK18mobsacB::Δ*bmoA*	pK18mobsacB carrying truncated *bmoA* (csal_1004) gene	This study
pK18mobsacB::Δ*bmoB*	pK18mobsacB carrying truncated *bmoB* (csal_1005) gene	This study
pBBR1MCS	Broad-host-range vector, Cm[r]	55
pBBR1MCS-bmoA	pBBR1MCS-2 carrying *bmoA* and its predicted native promoter region, Cm[r]	This study
pBBR1MCS-bmoB	pBBR1MCS carrying *bmoB* and its predicted native promoter region, Cm[r]	This study
pBBR1MCS-bmoA-bmoB	pBBR1MCS carrying *bmoA* and *bmoB* and their predicted native promoter regions, Cm[r]	This study
pACYCDuet1	Dual protein expression vector, Cm[r]	Novagen
pACYC-bmoA	pACYCDuet1 carrying *bmoA* in MCS-1 under the control of the T7 promoter, Cm[r]	This study
pACYC-bmoB	pACYCDuet1 carrying *bmoB* in MCS-2 under the control of the T7 promoter, Cm[r]	This study
pACYC-bmoA-bmoB	pACYCDuet1 carrying *bmoA* in MCS-1 and *bmoB* in MCS-2 under the control of their respective T7 promoters, Cm[r]	This study
pET-28a(+)	Expression vector, Km[r]	Novagen
pET28a-bmoA	pET28a carrying *bmoA* under the control of the T7 promoter (BmoA-His$_6$)	This study
pET28a-bmoB	pET28a carrying *bmoB* under the control of the T7 promoter (His$_6$-BmoB)	This study

[a]Cm[r], chloramphenicol resistant; Km[r], kanamycin resistant.
[b]DSMZ, German Collection of Microorganisms and Cell Cultures.

(sacB-F/sacB-R and either 1004-test-F/1004-test-R [for *bmoA*] or 1005-test-F/1005-test-R [for *bmoB*]) to verify the absence of vector sequences and the presence of the mutant allele in the chromosome of *C. salexigens*. The resultant *bmoA* and *bmoB* deletion mutants of *C. salexigens* ZW4-1 were named strains 3043Δ*bmoA* and 3043Δ*bmoB*, respectively.

Complementation assays. Complementation of *C. salexigens* strains 3043Δ*bmoA* and 3043Δ*bmoB* was performed by cloning full-length *bmoA* or *bmoB* along with its flanking DNA into the broad-host-range plasmid pBBR1MCS (chloramphenicol resistant [Cm[r]]) (55), in which the target gene is under the control of its native promoter, and the *E. coli* S17-1 strain was used to transfer the complementation plasmid into a *C. salexigens* deletion mutant by conjugation. For complementation of strain 3043Δ*bmoA*, a 1.7-kb fragment encompassing the wild-type *bmoA* and its surrounding DNA was amplified from the genomic DNA of ZW4-1 strain (Rif[r]) with the primers 04HF/04HR and cloned into the HindIII-BamHI sites of pBBR1MCS using the ClonExpress II one-step cloning kit (Vazyme, China); this yielded plasmid pBBR1MCS-bmoA, which contains the *bmoA* gene with its predicted native promoter (Fig. S3). For complementation of strain 3043Δ*bmoB*, a 1.4-kb fragment containing the wild-type *bmoB* and its surrounding DNA was amplified by PCR with the primers 05HF/05HR and ligated into the HindIII/BamHI sites of pBBBR1MCS, creating plasmid pBBR1MCS-bmoB (Fig. S3). DNA sequencing confirmed that the insertions in the plasmids were identical to the wild-type gene sequences. The complementation plasmid was transferred from *E. coli* S17-1 into the corresponding gene deletion mutants by conjugation, as described above. The gene complementary mutants were screened on D5 agar in the presence of Rif and Cm for strain 3043Δ*bmoA* carrying pBBR1MCS-bmoA and strain 3043Δ*bmoB* carrying pBBR1MCS-bmoB. The presence of plasmids in *C. salexigens* cells was verified by extraction of plasmids and gel electrophoresis. The abilities of complementation strains to use glucose, GB, or dimethylglycine as the sole carbon source were determined on C-M63 agar plates, while the wild type was used as the positive control and strains 3043Δ*bmoA*(pBBR1MCS) and 3043Δ*bmoB*(pBBR1MCS) as the negative controls.

Functional study of *bmoA* and *bmoB* in *E. coli*. Both the *bmoA* and *bmoB* genes were amplified by PCR from the genomic DNA of strain ZW4-1 with the primers listed in Table 4. The *bmoA* PCR product was digested by NcoI and HindIII and inserted into the NcoI/HindIII sites of the MCS1 position in pACYCDuet-1 to generate the plasmid pACYC-bmoA, while the *bmoB* PCR product was digested by NdeI and PvuI and cloned into the NdeI/PvuI sites of the MCS2 position in pACYCDuet-1 to generate the plasmid pACYC-bmoB. For coexpression of BmoA and BmoB, the NdeI-PvuI fragment from pACYC-bmoB was ligated into NdeI-PvuI-digested pACYC-bmoA, generating the plasmid pACYC-bmoA-bmoB. The three recombinant plasmids were individually transformed into the competent *E. coli* BL21(DE3) cells, and single colonies of the positive transformants were picked and inoculated into LB broth containing Cm with shaking at 180 rpm and 37°C. When the optical density at 600 nm (OD$_{600}$) reached 0.4 to 0.6, IPTG was added to induce protein expression (0.1 mM for BmoA, 0.05 mM for BmoB, and 0.1 mM for

TABLE 4 Primers used in this study

Primer	Sequence (5′ to 3′)[a]	Purpose
1004uF	CTATGACATGATTAC<u>GAATTC</u>ACGATTTGCCTTATTACCACC (EcoRI)	Amplification of upstream flanking region of *bmoA* for
1004uR	<u>GGATCC</u>CCTTCATTGCACATCGTTCA (BamHI)	construction of pK18mobsacB::Δ*bmoA*
1004dF	<u>GGATCC</u>GAGCAGATCCATGAAGGCAT (BamHI)	Amplification of downstream flanking region of *bmoA* for
1004dR	ACGACGGCCAGTGCC<u>AAGCTT</u>CCTCGTGATAGTGGCTCATG (HindIII)	construction of pK18mobsacB::Δ*bmoA*
1005uF	CTATGACATGATTAC<u>GAATTC</u>CCACCTTGACGTTATCCATC (EcoRI)	Amplification of upstream flanking region of *bmoB* for
1005uR	CATGACTCTTGAAGAAATTCTGGGTCATGGA	construction of pK18mobsacB::Δ*bmoB*
1005dF	GAATTTCTTCAAGAGTCATGTCGCCATCG	Amplification of downstream flanking region of *bmoB* for
1005dR	ACGACGGCCAGTGCC<u>AAGCTT</u>TGCCATCGTGTATGTGTCA (HindIII)	construction of pK18mobsacB::Δ*bmoB*
sacB-F	CGACAACCATACGCTGAGAG	Amplification of partial *sacB* gene fragment
sacB-R	CGAAGCCCAACCTTTCATA	
1004-test-F	TGAACGATGTGCAATGAAGG	Primers for screening of *bmoA* double-crossover mutant strains
1004-test-R	GCATACCCCATTCAATGTCA	
1005-test-F	TTCGTAGGTCCTGGAGTAGG	Primers for screening of *bmoB* double-crossover mutant strains
1005-test-R	CGATGGCGACATGACT	
04HF	GTCGACGGTATCGATAGGTATCCTCGCTCGGGCATT	Amplification of *bmoA* for construction of pBBR1MCS-bmoA
04HR	CGCTCTAGAACTAGTGGAAAGTCTACCTGGTCGC	
05HF	GTCGACGGTATCGATTGAATGGGGTATGCGTGA	Amplification of *bmoB* for construction of pBBR1MCS-bmoB
05HR	CGCTCTAGAACTAGTAGTCACGCTGAGCGCCC	
04EF	CATG<u>CCATGG</u>ATCTGCTCGCCACAT (NcoI)	Amplification of *bmoA* gene for construction of pET28a-bmoA
04ER	CCC<u>AAGCTT</u>GCCCTGAACGATGTGCAA (HindIII)	
05EF	CGC<u>CATATG</u>ACCCAGAATTTCTTCAATC (NdeI)	Amplification of *bmoB* gene for construction of pET28a-bmoB
05ER	CGC<u>GGATCC</u>TCAGAACTCGATGGCGAC (BamHI)	
04EF2	CATG<u>CCATGG</u>ATCTGCTCGCCACAT (NcoI)	Amplification of *bmoA* gene for construction of pACYC-bmoA
04ER2	CCC<u>AAGCTT</u>TCAGCCCTGAACGATGTG (HindIII)	
05EF2	CGC<u>CATATG</u>ACCCAGAATTTCTTCAATC (NdeI)	Amplification of *bmoB* gene for construction of pACYC-bmoB
05ER2	TCG<u>CGATCG</u>TCAGAACTCGATGGCGAC (PvuI)	

[a]Restriction sites are underlined and the restriction enzymes are in parentheses next to the sequence.

coexpression of BmoA and BmoB). After further incubation at 25°C for 40 h, the cells were harvested, washed twice with carbon-free C-M63 medium, and disrupted by sonication. The cell debris was removed by centrifugation, and the compatible solutes in the supernatant were extracted and detected by ^{13}C NMR spectroscopy, as described below.

Extraction of intracellular solutes and ^{13}C NMR analysis. Cells were pelleted by centrifugation and washed twice with the same carbon-free growth medium, and cellular solutes were extracted as described by Martins and Santos (56). Freeze-dried extracts were dissolved in 0.5 ml of D_2O and then placed into 5-mm nuclear magnetic resonance (NMR) tubes. Natural-abundance ^{13}C NMR spectra were recorded at 25°C with a Bruker Avance III HD 500 MHz superconducting FT NMR spectrometer at 125 MHz. ^{13}C chemical shifts were referenced to an external dimethyl sulfoxide standard (δ = 40.6 ppm) and assigned by comparison with those of standard compounds.

Expression and purification of His-tagged recombinant proteins. To express BmoA as a C-terminal histidine-tagged fusion protein, the coding region of *bmoA* gene was PCR amplified from ZW4-1 genomic DNA with the primers 04EF/04ER. The PCR products were digested with NcoI and HindIII, gel purified, and ligated into the same sites of pET28a, yielding pET28a-bmoA. To express BmoB as an N-terminal histidine-tagged fusion protein, the coding region of *bmoB* gene was PCR amplified with the primers 05EF/05ER, digested with NdeI and BamHI, and cloned into the same sites of pET28a, creating pET28a-bmoB. Subsequently, the expression vectors were separately transformed into *E. coli* BL21(DE3) competent cells. *E. coli* BL21(DE3) cells carrying pET28a-bmoA or pET28a-bmoB were aerobically cultured in LB broth containing Km, 100 μM Na_2S, and 50 μM $NH_4Fe(SO_4)_2$ with constant shaking (180 rpm) at 37°C until the OD_{600} values reached 0.4 to 0.6; at that time, isopropyl-β-D-thiogalactopyranoside (IPTG) was added (0.1 mM and 0.05 mM for BmoA and BmoB expression) to induce protein expression. After further incubation at 25°C for 16 h, cells were harvested by centrifugation, washed twice with 50 mM Tris-HCl (pH 7.0), and resuspended in the same buffer. Cells were disrupted by sonication for 30 min (200 W, 3-s pulsing and 6-s resting), followed by centrifugation at 6,000 $\times$ g for 15 min at 4°C. The recombinant proteins in the supernatant were purified with the Ni-NTA Sefinose resin kit (Sango, China), according to the manufacturer's protocol, further concentrated to 3 to 5 ml using Amicon Ultra 10-kDa molecular weight cutoff (MWCO) filters (Merck), and analyzed by sodium dodecyl sulfate-polyacrylamide gel electrophoresis (SDS-PAGE). The concentrations of the purified enzymes were quantified by the Bradford method (57) using bovine serum albumin (fraction V) as the standard.

Determination of molecular weights. The native molecular weights of BmoA-His$_6$ and His$_6$-BmoB were estimated by gel filtration chromatography on a Sephacryl S-200 high-resolution (HR) column (1.6 by 90 cm), which was calibrated with sweet potato β-amylase (molecular weight, 200,000), yeast alcohol dehydrogenase (150,000), bovine serum albumin (66,000), ovalbumin (43,000), and cytochrome *c* from horse heart (12,400). The column was preequilibrated and eluted with 50 mM Tris-HCl buffer (pH 7.0) containing 150 mM NaCl at a flow rate of 0.5 ml/min. The void volume (V_o) of the column was estimated using blue dextran (2,000 kDa), while the elution volume (V_e) for each protein was calculated from the midpoint of the peaks. The data were plotted in terms of log of molecular weight against V_e/V_o. The

molecular weights of the subunits of purified enzyme were estimated by sodium dodecyl sulfate-polyacrylamide gel electrophoresis (SDS-PAGE), as described previously (58).

Enzyme assays. (i) Flavin reductase activity assay. The flavin reductase activity of His_6-BmoB was monitored by measuring NADH consumption at 340 nm and calculated using the molar extinction coefficient of 6.22 $mM^{-1} \cdot cm^{-1}$. A typical reaction mixture contained 50 mM Tris-HCl (pH 7.0), 0.15 mM FAD, and 1.2 μM purified His_6-BmoB in a final volume of 1 ml. The reactions were started by adding 0.2 mM NADH to the reaction mixture. An assay mixture without FAD was used as a blank. One unit of reductase activity was defined as the amount of enzyme catalyzing the oxidation of 1 μmol NADH per minute at 25°C under the assay conditions. To determine the substrate specificity of BmoB, NADPH, FMN, and riboflavin were employed as the substrates.

The kinetic parameters of BmoB were determined by incubating the protein (1.2 μM) with various concentrations of tested substrates (NADH, NADPH, FMN, FAD, or riboflavin), as indicated in Table 1, in 50 mM Tris-HCl (pH 7.0) at 25°C. The absorption coefficients used in this study were the same as those described by Otto et al. (59). The kinetic experiments were performed with three different enzyme preparations, and apparent kinetic parameters were obtained using nonlinear regression analysis via the Michaelis-Menten equation in GraphPad Prism 5.

(ii) GB monooxygenase assay. Glycine betaine monooxygenase activity was assayed by measuring the amount of formaldehyde produced with the Nash reagent, as described previously (60), with some modifications. The standard reaction mixture contained 50 mM Tris-HCl (pH 7.0), 2 mM $FeSO_4$, 5 mM NADH, 10 μM FAD, 2 mM GB, 17 μM BomA-His_6, and 3.4 μM His_6-BmoB in a total volume of 1 ml. The reaction was started by adding NADH to the reaction mixture. After incubation at 30°C for 30 min with shaking, the reaction was stopped by addition of 0.1 ml of 75% (vol/vol) trichloroacetic acid, and denatured proteins were removed by centrifugation. The resultant supernatant was mixed with equal volume of Nash reagent and incubated for 50 min at 37°C for color development. Then, the absorbance was measured at 412 nm. One unit of activity was defined as the amount of enzyme required to produce 1 nmol formaldehyde per minute under the assay conditions. Specific activity was defined as the unit per milligram of protein.

Flavin determination and quantification. Noncovalent binding of the flavin cofactor present in BmoB was determined by trichloroacetic acid treatment, as described previously (61). Preparations of the purified His_6-BmoB were boiled for 10 min to release the flavin and then centrifuged to remove the denatured protein. The resultant supernatant was further filtered across a 0.45-μm nitrocellulose membrane, subjected to an Agilent 1100 series HPLC system equipped with an Agilent Zorbax SB-Aq C_{18} column (250 by 4.6 mm, 5 μm particle size), and eluted with a mobile phase consisting of a mixture of 20 mM ammonium acetate dissolved in water (pH 6.0) (91%) and acetonitrile (9%) at a flow rate of 1 ml/min, as described by Petrusma et al. (62). The column temperature was maintained at 30°C, and the detection wavelength was set at 375 nm. The eluent was identified by comparing the retention time and UV-visible spectra to those of the authentic FMN (retention time, 8.87 min) and FAD (retention time, 11.65 min). The FAD content of His6-BmoB was determined spectrophotometrically by using the molecular absorption coefficient of $\varepsilon_{450} = 11,300$ $M^{-1} \cdot cm^{-1}$ for free FAD (63).

Analysis of the reaction products. GB and dimethylglycine *in vitro* assays were measured by a HPLC system (Agilent 1100 series) with a Supelcosil LC-SCX column (25 cm by 4.6 mm, 5 μm; Supelco, Inc.), as described by Laryea et al. (64), with some modifications. The mobile phase was a 90% acetonitrile–10% choline aqueous solution (22 mM) at a flow rate of 1.5 ml $\cdot min^{-1}$. UV detection was set at a 254 nm wavelength. Under these assay conditions, the retention times of GB and dimethylglycine were determined to be 23.49 min and 21.18 min, respectively. Compounds were identified by comparison with the retention times and UV-visible spectra of authentic standards. Quantitation of GB and dimethylglycine in the reaction quench solution was accomplished by a comparison of the peak heights with those of external standards at known concentrations. The amount of hydrogen peroxide generated during the *in vitro* assays was measured using a horseradish peroxidase (HRP)-coupled oxidation reaction, as described previously (65).

Effects of metal ions and EDTA on BMO activity. The effects of metal ions and EDTA on BMO activity were determined by the addition of each metal ion (NaCl, KCl, $FeSO_4$, $MnSO_4$, $CuSO_4$, $ZnSO_4$, $MgCl_2$, $CaCl_2$, $CoCl_2$, and $AgNO_3$) or EDTA to the reaction mixture at a final concentration of 2 mM, and the enzyme activities were measured under standard conditions.

Determination of the content of iron and acid-labile sulfide. The total iron (66) and acid-labile sulfide (67) contents of enzymes were determined colorimetrically with tripyridyl-s-triazine and *N,N*-dimethyl-*p*-phenylenediamine, respectively.

Sequence and phylogenetic analysis. Nucleotide and deduced amino acid sequence similarity searches were carried out using the BLAST program (http://www.ncbi.nlm.nih.gov/BLAST). Multiple-sequence alignment analysis was performed with DNAMAN version 8.0. Phylogenetic trees of BmoA with the members in RO family were constructed using neighbor-joining algorithm in MEGA 7.0 (68). Confidence for tree topology was estimated based on 1,000 bootstrap replicates.

SUPPLEMENTAL MATERIAL

Supplemental material for this article may be found at https://doi.org/10.1128/AEM .00377-18.

SUPPLEMENTAL FILE 1, PDF file, 0.9 MB.

ACKNOWLEDGMENTS

REFERENCES

1. Welsh DT. 2000. Ecological significance of compatible solute accumulation by micro-organisms: from single cells to global climate. FEMS Microbiol Rev 24:263–290. https://doi.org/10.1111/j.1574-6976.2000.tb00542.x.

2. Ziegler C, Bremer E, Krämer R. 2010. The BCCT family of carriers: from physiology to crystal structure. Mol Microbiol 78:13–34. https://doi.org/10.1111/j.1365-2958.2010.07332.x.

3. Pao SS, Paulsen IT, Saier MH, Jr. 1998. Major facilitator superfamily. Microbiol Mol Biol Rev 62:1–34.

4. Boscari A, Mandon K, Poggi M-C, Le Rudulier D. 2004. Functional expression of *Sinorhizobium meliloti* BetS, a high-affinity betaine transporter, in *Bradyrhizobium japonicum* USDA110. Appl Environ Microbiol 70:5916–5922. https://doi.org/10.1128/AEM.70.10.5916-5922.2004.

5. Chen C, Malek AA, Wargo MJ, Hogan DA, Beattie GA. 2010. The ATP-binding cassette transporter Cbc (choline/betaine/carnitine) recruits multiple substrate-binding proteins with strong specificity for distinct quaternary ammonium compounds. Mol Microbiol 75:29–45. https://doi.org/10.1111/j.1365-2958.2009.06962.x.

6. Nyyssölä A, Kerovuo J, Kaukinen P, von Weymarn N, Reinikainen T. 2000. Extreme halophiles synthesize betaine from glycine by methylation. J Biol Chem 275:22196–22201. https://doi.org/10.1074/jbc.M910111199.

7. Nyyssölä A, Reinikainen T, Leisola M. 2001. Characterization of glycine sarcosine *N*-methyltransferase and sarcosine dimethylglycine *N*-methyltransferase. Appl Environ Microbiol 67:2044–2050. https://doi.org/10.1128/AEM.67.5.2044-2050.2001.

8. Oren A. 1990. Formation and breakdown of glycine betaine and trimethylamine in hypersaline environments. Antonie Van Leeuwenhoek 58:291–298. https://doi.org/10.1007/BF00399342.

9. Müller E, Fahlbusch K, Walther R, Gottschalk G. 1981. Formation of *N,N*-dimethylglycine, acetic acid, and butyric acid from betaine by *Eubacterium limosum*. Appl Environ Microbiol 42:439–445.

10. Kortstee GJJ. 1970. The aerobic decomposition of choline by microorganisms. Arch Mikrobiol 71:235–244. https://doi.org/10.1007/BF00410157.

11. Časaitė V, Povilonienė S, Meškienė R, Rutkienė R, Meškys R. 2011. Studies of dimethylglycine oxidase isoenzymes in *Arthrobacter globiformis* cells. Curr Microbiol 62:1267–1273. https://doi.org/10.1007/s00284-010-9852-6.

12. Chlumsky LJ, Zhang L, Jorns MS. 1995. Sequence analysis of sarcosine oxidase and nearby genes reveals homologies with key enzymes of folate one-carbon metabolism. J Biol Chem 270:18252–18259. https://doi.org/10.1074/jbc.270.31.18252.

13. Boncompagni E, Osteras M, Poggi MC, le Rudulier D. 1999. Occurrence of choline and glycine betaine uptake and metabolism in the family *Rhizobiaceae* and their roles in osmoprotection. Appl Environ Microbiol 65:2072–2077.

14. Vargas C, Jebbar M, Carrasco R, Blanco C, Calderón MI, Iglesias-Guerra F, Nieto JJ. 2006. Ectoines as compatible solutes and carbon and energy sources for the halophilic bacterium *Chromohalobacter salexigens*. J Appl Microbiol 100:98–107. https://doi.org/10.1111/j.1365-2672.2005.02757.x.

15. White RF, Kaplan L, Birnbaum J. 1973. Betaine-homocysteine transmethylase in *Pseudomonas denitrificans*, a vitamin B_{12} overproducer. J Bacteriol 113:218–223.

16. Smith LT, Pocard JA, Bernard T, Le Rudulier D. 1988. Osmotic control of glycine betaine biosynthesis and degradation in *Rhizobium meliloti*. J Bacteriol 170:3142–3149. https://doi.org/10.1128/jb.170.7.3142-3149.1988.

17. Barra L, Fontenelle C, Ermel G, Trautwetter A, Walker GC, Blanco C. 2006. Interrelations between glycine betaine catabolism and methionine biosynthesis in *Sinorhizobium meliloti* strain 102F34. J Bacteriol 188:7195–7204. https://doi.org/10.1128/JB.00208-06.

18. Waditee R, Incharoensakdi A. 2001. Purification and kinetic properties of betaine-homocysteine methyltransferase from *Aphanothece halophytica*. Curr Microbiol 43:107–111. https://doi.org/10.1007/s002840010270.

19. Wargo MJ, Szwergold BS, Hogan DA. 2008. Identification of two gene clusters and a transcriptional regulator required for *Pseudomonas aeruginosa* glycine betaine catabolism. J Bacteriol 190:2690–2699. https://doi.org/10.1128/JB.01393-07.

20. Li S, Yu X, Beattie GA. 2013. Glycine betaine catabolism contributes to *Pseudomonas syringae* tolerance to hyperosmotic stress by relieving betaine-mediated suppression of compatible solute synthesis. J Bacteriol 195:2415–2423. https://doi.org/10.1128/JB.00094-13.

21. Fitzsimmons LF, Hampel KJ, Wargo MJ. 2012. Cellular choline and glycine betaine pools impact osmoprotection and phospholipase C production in *Pseudomonas aeruginosa*. J Bacteriol 194:4718–4726. https://doi.org/10.1128/JB.00596-12.

22. Copeland A, O'Connor K, Lucas S, Lapidus A, Berry KW, Detter JC, Del Rio TG, Hammon N, Dalin E, Tice H, Pitluck S, Bruce D, Goodwin L, Han C, Tapia R, Saunders E, Schmutz J, Brettin T, Larimer F, Land M, Hauser L, Vargas C, Nieto JJ, Kyrpides NC, Ivanova N, Göker M, Klenk HP, Csonka LN, Woyke T. 2011. Complete genome sequence of the halophilic and highly halotolerant *Chromohalobacter salexigens* type strain (1H11ᵀ). Stand Genomic Sci 5:379–388. https://doi.org/10.4056/sigs.2285059.

23. Shao Y-H, Guo L-Z, Yu H, Zhao B-S, Lu W-D. 2017. Establishment of a markerless gene deletion system in *Chromohalobacter salexigens* DSM 3043. Extremophiles 21:839–850. https://doi.org/10.1007/s00792-017-0946-y.

24. Daughtry KD, Xiao Y, Stoner-Ma D, Cho E, Orville AM, Liu P, Allen KN. 2012. Quaternary ammonium oxidative demethylation: X-ray crystallographic, resonance Raman, and UV-visible spectroscopic analysis of a Rieske-type demethylase. J Am Chem Soc 134:2823–2834. https://doi.org/10.1021/ja2111898.

25. Kauppi B, Lee K, Carredano E, Parales RE, Gibson DT, Eklund H, Ramaswamy S. 1998. Structure of an aromatic-ring-hydroxylating dioxygenase-naphthalene 1,2-dioxygenase. Structure 6:571–586. https://doi.org/10.1016/S0969-2126(98)00059-8.

26. Calderón MI, Vargas C, Rojo F, Iglesias-Guerra F, Csonka LN, Ventosa A, Nieto JJ. 2004. Complex regulation of the synthesis of the compatible solute ectoine in the halophilic bacterium *Chromohalobacter salexigens* DSM 3043ᵀ. Microbiology 150:3051–3063. https://doi.org/10.1099/mic.0.27122-0.

27. Reese MG. 2001. Application of a time-delay neural network to promoter annotation in the *Drosophila melanogaster* genome. Comput Chem 26:51–56. https://doi.org/10.1016/S0097-8485(01)00099-7.

28. Galinski EA. 1995. Osmoadaptation in bacteria. Adv Microb Physiol 37:273–328. https://doi.org/10.1016/S0065-2911(08)60148-4.

29. May G, Faatz E, Villarejo M, Bremer E. 1986. Binding protein dependent transport of glycine betaine and its osmotic regulation in *Escherichia coli* K12. Mol Gen Genet 205:225–233. https://doi.org/10.1007/BF00430432.

30. Lee J, Simurdiak M, Zhao H. 2005. Reconstitution and characterization of aminopyrrolnitrin oxygenase, a Rieske *N*-oxygenase that catalyzes unusual arylamine oxidation. J Biol Chem 280:36719–36727. https://doi.org/10.1074/jbc.M505334200.

31. Eichhorn E, van der Ploeg JR, Leisinger T. 1999. Characterization of a two-component alkanesulfonate monooxygenase from *Escherichia coli*. J Biol Chem 274:26639–26646. https://doi.org/10.1074/jbc.274.38.26639.

32. Rosche B, Tshisuaka B, Fetzner S, Lingens F. 1995. 2-Oxo-1,2-dihydroquinoline 8-monooxygenase, a two-component enzyme system from *Pseudomonas putida* 86. J Biol Chem 270:17836–17842. https://doi.org/10.1074/jbc.270.30.17836.

33. Cafaro V, Scognamiglio R, Viggiani A, Izzo V, Passaro I, Notomista E, Piaz FD, Amoresano A, Casbarra A, Pucci P, Di Donato A. 2002. Expression and purification of the recombinant subunits of toluene/*o*-xylene monooxygenase and reconstitution of the active complex. Eur J Biochem 269:5689–5699. https://doi.org/10.1046/j.1432-1033.2002.03281.x.

34. Bill E, Bernhardt F-H, Trautwein AX. 1981. Mössbauer studies on the active Fe . . .[2Fe-2S] site of putidamonooxin, its electron transport and dioxygen activation mechanism. Eur J Biochem 121:39–46. https://doi .org/10.1111/j.1432-1033.1981.tb06426.x.

35. Burnet M, Lafontaine PJ, Hanson AD. 1995. Assay, purification, and partial characterization of choline monooxygenase from spinach. Plant Physiol 108:581–588. https://doi.org/10.1104/pp.108.2.581.

36. Chaiyen P, Suadee C, Wilairat P. 2001. A novel two-protein component flavoprotein hydroxylase. Eur J Biochem 268:5550–5561. https://doi.org/ 10.1046/j.1432-1033.2001.02490.x.

37. Lei B, Tu SC. 1998. Mechanism of reduced flavin transfer from Vibrio harveyi NADPH-FMN oxidoreductase to luciferase. Biochemistry 37: 14623–14629. https://doi.org/10.1021/bi981841+.

38. Bernhardt F-H, Bill E, Trautwein AX, Twilfer H. 1988. 4-Methoxybenzoate monooxygenase from Pseudomonas putida: isolation, biochemical properties, substrate specificity, and reaction mechanisms of the enzyme components. Methods Enzymol 161:281–294. https://doi.org/10.1016/ 0076-6879(88)61031-7.

39. Dumitru R, Jiang WZ, Weeks DP, Wilson MA. 2009. Crystal structure of dicamba monooxygenase: a Rieske nonheme oxygenase that catalyzes oxidative demethylation. J Mol Biol 392:498–510. https://doi.org/10 .1016/j.jmb.2009.07.021.

40. van der Geize R, Hessels GI, van Gerwen R, van der Meijden P, Dijkhuizen L. 2002. Molecular and functional characterization of kshA and kshB, encoding two components of 3-ketosteroid 9α-hydroxylase, a class IA monooxygenase, in Rhodococcus erythropolis strain SQ1. Mol Microbiol 45:1007–1018. https://doi.org/10.1046/j.1365-2958.2002.03069.x.

41. Rosche B, Tshisuaka B, Hauer B, Lingens F, Fetzner S. 1997. 2-Oxo-1,2-dihydroquinoline 8-monooxygenase: phylogenetic relationship to other multicomponent nonheme iron oxygenases. J Bacteriol 179:3549–3554. https://doi.org/10.1128/jb.179.11.3549-3554.1997.

42. Burnet MW, Goldmann A, Message B, Drong R, El Amrani A, Loreau O, Slightom J, Tepfer D. 2000. The stachydrine catabolism region in Sinorhizobium meliloti encodes a multi-enzyme complex similar to the xenobiotic degrading systems in other bacteria. Gene 244:151–161. https://doi .org/10.1016/S0378-1119(99)00554-5.

43. Karlsson A, Beharry ZM, Matthew Eby D, Coulter ED, Neidle EL, Kurtz DM, Jr, Eklund H, Ramaswamy S. 2002. X-ray crystal structure of benzoate 1,2-dioxygenase reductase from Acinetobacter sp. strain ADP1. J Mol Biol 318:261–272. https://doi.org/10.1016/S0022-2836(02)00039-6.

44. Batie CJ, Ballou DP, Correll CC. 1991. Phthalate dioxygenase reductase and related flavin-iron-sulfur containing electron transferases. Chem Biochem Flavoenzymes 3:543–556.

45. Zhu Y, Jameson E, Crosatti M, Schafer H, Rajakumar K, Bugg TD, Chen Y. 2014. Carnitine metabolism to trimethylamine by an unusual Rieske-type oxygenase from human microbiota. Proc Natl Acad Sci U S A 111:4268–4273. https://doi.org/10.1073/pnas.1316569111.

46. Ertekin E, Konstantinidis KT, Tezel U. 2017. A Rieske-type oxygenase of Pseudomonas sp. BIOMIG1 converts benzalkonium chlorides to benzyldimethyl amine. Environ Sci Technol 51:175–181. https://doi.org/10.1021/ acs.est.6b03705.

47. Correll CC, Batie CJ, Ballou DP, Ludwig ML. 1985. Crystallographic characterization of phthalate oxygenase reductase, an iron-sulfur flavoprotein from Pseudomonas cepacia. J Biol Chem 260:14633–14635.

48. Capyk JK, Eltis LD. 2012. Phylogenetic analysis reveals the surprising diversity of an oxygenase class. J Biol Inorg Chem 17:425–436. https:// doi.org/10.1007/s00775-011-0865-9.

49. Nam J-W, Nojiri H, Yoshida T, Habe H, Yamane H, Omori T. 2001. New classification system for oxygenase components involved in ring-hydroxylating oxygenations. Biosci Biotechnol Biochem 65:254–263. https://doi.org/10.1271/bbb.65.254.

50. Pinto A, Tarasev M, Ballou DP. 2006. Substitutions of the "bridging" aspartate 178 result in profound changes in the reactivity of the Rieske center of phthalate dioxygenase. Biochemistry 45:9032–9041. https://doi .org/10.1021/bi060216z.

51. Parales RE, Parales JV, Gibson DT. 1999. Aspartate 205 in the catalytic domain of naphthalene dioxygenase is essential for activity. J Bacteriol 181:1831–1837.

52. Sambrook J, Fritsch EF, Maniatis T. 1989. Molecular cloning: a laboratory manual, 2nd ed. Cold Spring Harbor Laboratory Press, Cold Spring Harbor, NY.

53. Heckman KL, Pease LR. 2007. Gene splicing and mutagenesis by PCR-driven overlap extension. Nat Protoc 2:924–932. https://doi.org/10 .1038/nprot.2007.132.

54. Schäfer A, Tauch A, Jäger W, Kalinowski J, Thierbach G, Pühler A. 1994. Small mobilizable multi-purpose cloning vectors derived from the Escherichia coli plasmids pK18 and pK19: selection of defined deletions in the chromosome of Corynebacterium glutamicum. Gene 145:69–73. https:// doi.org/10.1016/0378-1119(94)90324-7.

55. Kovach ME, Elzer PH, Steven Hill D, Robertson GT, Farris MA, Roop RM, II, Peterson KM. 1995. Four new derivatives of the broad-host-range cloning vector pBBR1MCS, carrying different antibiotic-resistance cassettes. Gene 166:175–176. https://doi.org/10.1016/0378-1119(95)00584-1.

56. Martins LO, Santos H. 1995. Accumulation of mannosylglycerate and di-myo-inositol-phosphate by Pyrococcus furiosus in response to salinity and temperature. Appl Environ Microbiol 61:3299–3303.

57. Bradford MM. 1976. A rapid and sensitive method for the quantitation of microgram quantities of protein utilizing the principle of protein-dye binding. Anal Biochem 72:248–254. https://doi.org/10 .1016/0003-2697(76)90527-3.

58. Laemmli UK. 1970. Cleavage of structural proteins during the assembly of the head of bacteriophage T4. Nature 227:680. https://doi.org/10 .1038/227680a0.

59. Otto K, Hofstetter K, Rothlisberger M, Witholt B, Schmid A. 2004. Biochemical characterization of StyAB from Pseudomonas sp. strain VLB120 as a two-component flavin-diffusible monooxygenase. J Bacteriol 186: 5292–5302. https://doi.org/10.1128/JB.186.16.5292-5302.2004.

60. Kleeberg U, Klinger W. 1982. Sensitive formaldehyde determination with NASH's reagent and a 'tryptophan reaction.' J Pharmacol Methods 8:19–31. https://doi.org/10.1016/0160-5402(82)90004-3.

61. Siegel LM. 1978. Quantitative determination of noncovalently bound flavins: types and methods of analysis. Methods Enzymol 53:419–429. https://doi.org/10.1016/S0076-6879(78)53046-2.

62. Petrusma M, Dijkhuizen L, van der Geize R. 2009. Rhodococcus rhodochrous DSM 43269 3-ketosteroid 9α-hydroxylase, a two-component iron-sulfur-containing monooxygenase with subtle steroid substrate specificity. Appl Environ Microbiol 75:5300–5307. https://doi.org/10.1128/ AEM.00066-09.

63. Kim E-M, Kim J, Seo J-H, Park J-S, Kim D-H, Kim B-G. 2012. Identification and characterization of the Rhizobium sp. strain GIN611 glycoside oxidoreductase resulting in the deglycosylation of ginsenosides. Appl Environ Microbiol 78:242–249. https://doi.org/10.1128/AEM.06404-11.

64. Laryea MD, Steinhagen F, Pawliczek S, Wendel U. 1998. Simple method for the routine determination of betaine and N,N-dimethylglycine in blood and urine. Clin Chem 44:1937–1941.

65. Seki M, Iida K, Saito M, Nakayama H, Yoshida S. 2004. Hydrogen peroxide production in Streptococcus pyogenes: involvement of lactate oxidase and coupling with aerobic utilization of lactate. J Bacteriol 186: 2046–2051. https://doi.org/10.1128/JB.186.7.2046-2051.2004.

66. Fischer DS, Price DC. 1964. A simple serum iron method using the new sensitive chromogen tripyridyl-s-triazine. Clin Chem 10:21–31. https:// doi.org/10.1016/0009-8981(64)90210-4.

67. Beinert H. 1983. Semi-micro methods for analysis of labile sulfide and of labile sulfide plus sulfane sulfur in unusually stable iron-sulfur proteins. Anal Biochem 131:373–378. https://doi.org/10.1016/0003 -2697(83)90186-0.

68. Kumar S, Stecher G, Tamura K. 2016. MEGA7: molecular evolutionary genetics analysis version 7.0 for bigger datasets. Mol Biol Evol 33: 1870–1874. https://doi.org/10.1093/molbev/msw054.